

Galaxy evolution in nearby loose groups. II. Photometric and kinematic characterization of USGC U268 and USGC U376 group members in the Leo cloud*

A. Marino^{1†}, H. Plana², R. Rampazzo³, L. Bianchi⁴, M. Rosado⁵, D. Bettoni³,
G. Galletta¹, P. Mazzei³, L. Buson³, P. Ambrocio-Cruz⁶, R. F. Gabbasov⁵

¹*Dipartimento di Fisica e Astronomia G. Galilei di Padova, vicolo dell'Osservatorio 3, I-35122 Padova, Italy*

²*Laboratorio de Astrofísica Teórica e Observacional, Universidade Estadual de Santa Cruz, Rodovia Ilhéus-Itabuna Km 16 45650-000 Ilhéus - BA, Brazil*

³*INAF-Osservatorio Astronomico di Padova, vicolo dell'Osservatorio 5, I-35122 Padova, Italy*

⁴*Dept. of Physics and Astronomy, Johns Hopkins University, 3400 North Charles Street, Baltimore, MD 21218 USA*

⁵*Instituto de Astronomía, Universidad Nacional Autónoma de México, Av. Universidad 3000, Ciudad Universitaria, C.P. 04510 México D.F., México*

⁶*Universidad Autónoma del Estado de Hidalgo, Área Académica de Ciencias de la Tierra y Materiales Ciudad Universitaria, Km 4.5 Carretera Pachuca - Tulancingo; Col. Carboneras C.P. 42184, Mineral de la Reforma, Hidalgo, México*

Accepted. Received

ABSTRACT

The paper is the second of a series in which we are exploring the co-evolution of galaxies and groups in the Local Universe, adopting a multi-wavelength approach. Here we present the photometric and kinematic characterization of two groups, USGC U268 and USGC U376 (U268 and U376 hereafter) located in different regions of the Leo cloud. We revisit the group membership, using results coming from recent redshift surveys, and we investigate their substructures. U268, composed of 10 catalogued members and 11 new added members, has a small fraction ($\approx 24\%$) of early-type galaxies (ETGs). U376 has 16 plus 8 new added members, with $\approx 38\%$ of ETGs. We find the presence of significant substructures in both groups suggesting that they are likely accreting galaxies. U268 is located in a more loose environment than U376. For each member galaxy, broad band integrated and surface photometry have been obtained in far-UV (FUV) and near-UV (NUV) with *GALEX*, and in u, g, r, i, z (SDSS) bands. H_α imaging and 2D high resolution kinematical data have been obtained using PUMA Scanning Fabry-Perot interferometer at the 2.12 m telescope in San Pedro Mártir, (Baja California, México). We improved the galaxy classification and we detected morphological and kinematical distortions that may be connected to either on-going and/or past interaction/accretion events or environmental induced secular evolution. U268 appears more active than U376, with a large fraction of galaxies showing interaction signatures (60% vs. 13%). The presence of bars among late-type galaxies is $\approx 10\%$ in U268 and $\approx 29\%$ in U376. The cumulative distribution of (FUV - NUV) colours of galaxies in U268 is significantly different than that in U376 with galaxies in U268 bluer than those in U376. In the ($FUV - r$ vs. M_r) and ($NUV - r$ vs. M_r) planes no members of U268 are found in the ‘red sequence’, even early-type galaxies lie in the ‘blue sequence’ or in the ‘green valley’. Most (80%) of the early-type members in U376 inhabit the ‘red sequence’, a large fraction of galaxies, of different morphological types, are located in the ‘green valley’, while the ‘blue sequence’ is under-populated with respect to U268.

Key words: galaxies: evolution – galaxies: groups: individual: USGC U268, USGC U376 – galaxies: photometry – ultraviolet: galaxies – galaxies: kinematics and dynamics

* Based on *GALEX* (GI6-6017, PI A. Marino) and PUMA (PI M. Rosado) observations. † E-mail:antonina.marino@unipd.it

1 INTRODUCTION

In the Local Universe, the distribution of galaxies is bimodal in the color space and relates to galaxy morphology (e.g. Strateva et al. 2001; Balogh et al. 2004). In the ($u - r$) vs. M_r color magnitude diagram (CMD), early-type quiescent galaxies populate the ‘red sequence’ and late-types, with active star formation, the blue one (e.g. Baldry et al. 2004). This bimodality is ubiquitous, extending from the general field, to groups and to clusters (e.g. Lewis et al. 2002). The physical origin of this bimodality is still under debate. However, there are strong evidences that the two distinct populations are the result of transformations driven by the environment. The galaxy evolution from the blue to the ‘red sequence’, i.e. from star forming to quiescent galaxies, occurs via transition that leads galaxies in an intermediate zone of the CMD, the ‘green valley’ (Martin et al. 2007). Since the color bimodality is mainly driven by the *on-off* of star formation activity and the UV bands are an excellent tracer of recent star formation, it is not surprising that the galaxy color sequences are especially well separated in the UV vs. optical CMD (e.g. Wyder et al. 2007). Investigating the mechanisms governing the *on-off* of the star formation in different environments is one of the main topic of the observational cosmology. In this respect, galaxy groups are important mainly from two facts. First, they contain a large fraction (~ 50 -60%) of the galaxies in the Local Universe (e.g. Geller & Huchra 1983; Tully 1988; Ramella et al. 2002; Eke et al. 2004; Tago et al. 2008). Second, since the galaxy velocity dispersion in groups is comparable to the inner velocity dispersion of individual galaxies, severe galaxy-galaxy interaction, accretions and merging are favoured in groups with respect to clusters (e.g. Mamon 1992; Schweizer 1996; Zabludoff & Mulchaey 1998a). Interactions, accretions and mergers **induce star formation (e.g. Kennicutt et al. 1996; Ellison et al. 2008, 2010; Scudder et al. 2012)**. The fraction of star-forming galaxies in groups lies between clusters ($< 30\%$) and field ($> 30\%$) (Calvi et al. 2012). This fact suggests the existence of pre-processing mechanisms acting on galaxies during the formation/virialization of groups, partly quenching star formation by ejecting the interstellar medium via starburst, AGN or shock-driven winds (e.g. Di Matteo et al. 2005) well before a group eventually fall into a cluster (see e.g. Zabludoff & Mulchaey 1998a; Bai et al. 2010, and references therein). Ram-pressure stripping phenomena may also have a role e.g. in removing the hot gas halos (Rasmussen et al. 2006; Kawata & Mulchaey 2008; McCarthy et al. 2008) i.e. the fuel for possible future star formation. Galaxy-galaxy interaction, accretions, and merging, ultimately control the members’ morphology (Toomre & Toomre 1972; Barnes 1996, 2002) typically turning late-type galaxies into ETGs. When and how the disks are transformed in spheroids, the star formation is quenched and stellar mass is accreted in the massive galaxies need to be further investigated.

In spite of the fact that groups are the most common environmental phase experienced by galaxies, and able to affect galaxy populations until transform their morphology, our understanding of the groups is still scarce. We intend to map the different forms of interactions within groups with the aim of investigating the co-evolution of groups and their members. This requires a considerable observational effort,

starting from the group definition, considering the presence of possible substructures, and a correct galaxy morphological (and kinematical) classification. Multi-wavelength surface photometric and 2D kinematical studies are necessary to identify the effect of interaction and accretion events, i.e. the main galaxy transforming mechanisms, as well as the secular evolution and to map their effect on the UV-optical CMDs.

In this context, we use Galaxy Evolution Explorer (*GALEX*) and Digital Sky Survey (SDSS) imaging to analyze a set of groups likely spanning a wide range of evolutionary phases, from analog to the Local Group to systems totally virialized (Marino et al. in prep.). We already presented a first study of three groups dominated by late-type galaxies in Marino et al. (2010, hereafter Paper I).

Here we present the UV and optical observations and the data analysis of two galaxy groups in the Leo cloud (Tully 1988). We focus in particular on U268 and U376. Starting from their definition given in Ramella et al. (2002) which identify bright group members, we revisit the two groups including fainter members, provided by recent redshift surveys, sharing the same spatial and velocity extent. For each galaxy group we investigate morphology, measure surface photometry in the UV, and optical bands and obtain UV - optical CMDs. We also achieved 2D $H\alpha$ data cubes for a fraction¹ of their bright late-type members.

The paper is arranged as follows. Section 2 describes the characteristics of the sample. Section 3 presents the photometric and kinematics observations and the data reduction. The photometric and kinematic results are presented in Section 4. The results are discussed and summarised in Sections 5 and 6 respectively. $H_0=75 \text{ km s}^{-1}\text{Mpc}^{-1}$ is used throughout the paper.

2 SAMPLE

The group sample has been selected from the catalog of Ramella et al. (2002) which lists 1168 groups of galaxies covering 4.69 steradians to a limiting magnitude of $m_B \approx 15.5$. In order to make a detailed morphological and photometric analysis, we have chosen only groups within 40 Mpc ($V_{hel} < 3000 \text{ km s}^{-1}$), and composed of at least 8 galaxies, **to map from intermediate to rich groups**, minimizing contamination by interlopers and spurious galaxies.

The cross-match of the member galaxies of the catalog with the *GALEX* and Sloan Digital Sky Survey (SDSS, York et al. (2000)) archives led to a sample of 13 nearby groups having almost of the members covered by both surveys. We further obtained new NUV imaging of most of the remaining galaxies in the *GALEX* GI6 (program 017). The sample contains groups having between 8 and 47 members, and a fraction of ETGs, according to the Hyper-Lyon-Meudon Extragalactic DAtabase (HYPERLEDA hereafter) (Paturel et al. 1997) classification, varying from those found in the field to $\approx 70\%$, typical of dense environments. The analysis of the entire sample will be presented in a forthcoming paper.

Here, we focus on 2 of the above groups, namely U268

¹ Since these observations are very time consuming.

Table 1. Characteristics of the galaxy members^a.

Group Galaxies	RA (J2000) [h:m:s]	Dec. (J2000) [d:m:s]	Morph. type	RC3 type	E(B-V) ^b [mag]	Incl. [deg]	logD ₂₅ [log(0.1 arcmin)]	logr ₂₅	P.A. [deg]	Mean Hel. Vel [km/s]	B _T [AB mag]
U268											
MRK 0408	09 48 04.8	+32 52 58	S0 ^f	-2.0	0.017	40.5	0.84	0.11	163.9	1470±40 ^c	14.84±0.48
NGC 3003	09 48 35.7	+33 25 17	Sbc	4.3	0.013	90.0	1.68	0.65	78.3	1498±36 ^c	12.09±0.10
NGC 3011	09 49 41.2	+32 13 16	S0	-1.8	0.016	38.6	0.92	0.08	59.5	1548±36 ^c	14.38±0.44
UGC 05287	09 51 28.1	+32 56 35	Sc	5.9	0.014	41.2	0.98	0.12	15 ^e	1482±42 ^c	14.68±0.42
UGC 05326	09 55 24.5	+33 15 47	IB	9.8	0.016	16.9	0.97	0.02	0 ^d	1415±45 ^c	14.46±0.40
IC 2524	09 57 33.0	+33 37 11	S0-a	-1.0	0.013	63.1	0.87	0.23	61.8	1487±10 ^c	14.84±0.49
NGC 3067	09 58 21.3	+32 22 11	SABa	2.1	0.015	81.8	1.31	0.49	104.3	1491±36 ^c	12.57±0.12
UGC 05393	10 01 42.1	+33 08 12	SBd	8.0	0.013	68.8	1.14	0.28	117.0	1448±25 ^c	14.79±0.38
UGC 05446	10 06 30.9	+32 56 49	Sc	5.9	0.014	80.5	1.12	0.61	49.8	1383±42 ^c	15.22±0.40
NGC 3118	10 07 11.6	+33 01 40	Sbc	4.1	0.018	90.0	1.32	0.67	38.6	1315±37 ^c	14.18±0.35
PGC2016633#	09 48 02.68	+32 54 01.7			0.016	53.1	0.63	0.21	165.0	1552±47	17.09±0.50
SDSSJ094838.45+332529.1*#	09 48 38.45	+33 25 29.1							86.8	1419±31	
PGC2042146#	09 49 03.1	+33 59 28.95			0.010	44.5	0.50	0.14	53.8	1494±2	17.69±0.50
SDSSJ094911.28+342634.2#	09 49 11.28	+34 26 34.2			0.012				164.1	1489±2	
SDSSJ094935.09+342616.3#	09 49 35.09	+34 26 16.3			0.010				98.3	1488±2	
PGC082546#	09 50 20.9	+33 35 02	Sc	4.6	0.015	46.3	0.56	0.15	171.0	1586±29	16.89±0.36
NGC3021#	09 50 57.1	+33 33 13	Sbc	4.0	0.014	55.7	1.13	0.23	108.3	1540±3	12.38± 0.27
SDSSJ095058.02+333319.3*#	09 50 58.02	+33 33 19.3			0.014				125.7	1596±3	
UGC05282#	09 51 10.4	+33 07 53	Sm	8.8	0.014	67.6	0.97	0.27	46.0	1557±10	
PGC2025214#	09 53 45.2	+33 09 52.0			0.013	57.2	0.55	0.25	18.5	1520±35	17.92± 0.50
SDSSJ095430.02+320342.0#	09 54 30.02	+32 03 42.0							152.9	1421±2	
SDSSJ100309.92+323622.5#	10 03 09.92	+32 36 22.5			0.015				123.3	1562±96	
SDSSJ100714.59+330221.5*#	10 07 14.59	+33 02 21.5							32.5	1252±4	
PGC029522#	10 08 58.0	+32 00 38	Sc	4.7	0.018	57.7	0.66	0.25	11.8	1468±34	16.75± 0.44
U376											
NGC 3592	11 14 27.5	+17 15 34	Sc	5.3	0.015	79.4	1.33	0.57	117.3	1298±20 ^c	14.31±0.30
NGC 3599	11 15 27.0	+18 06 37	S0	-2.0	0.021	28.3	1.38	0.04	0 ^d	812±31 ^c	12.72±0.08
NGC 3605	11 16 46.6	+18 01 01	E	-4.5	0.021	90.0	1.10	0.24	19.1	695±39 ^c	13.00±0.28
UGC 06296	11 16 51.0	+17 47 55 ^b	I	10.0	0.019	90.0	1.11	0.48	168.0	909±26 ^c	14.02±0.41
NGC 3607	11 16 54.7	+18 03 06	E-SO	-3.1	0.021	34.9	1.66	0.06	120.0	955±41 ^c	10.77±0.17
NGC 3608	11 16 59.0	+18 08 55	E	-4.8	0.021	47.0	1.50	0.08	80.0	1199±42 ^c	11.41±0.26
CGCG 096-024	11 17 58.0	+17 26 29			0.020	28.9	0.94	0.06	157.3	807±66 ^c	14.94±0.29
UGC 06320	11 18 17.5	+18 50 48			0.023	20.3	1.13	0.03	0 ^d	1125±5 ^c	13.67±0.41
UGC 06324	11 18 22.1	+18 44 18	S0	-1.9	0.022	90.0	1.14	0.33	166.8	1068±38 ^c	14.61±0.32
NGC 3626	11 20 03.9	+18 21 24	S0-a	-1.0	0.020	56.1	1.47	0.18	156.3	1570±37 ^c	11.64±0.23
NGC 3655	11 22 54.7	+16 35 24	Sc	5.0	0.025	47.1	1.18	0.16	31.8	1490±39 ^c	12.16±0.07
NGC 3659	11 23 45.3	+17 49 05	SBd	7.8	0.019	68.8	1.29	0.28	59.2	1282±39 ^c	12.76±0.48
NGC 3681	11 26 29.8	+16 51 48	Sbc	4.0	0.026	15.2	1.24	0.01	0 ^d	1236±53 ^c	12.26±0.16
NGC 3684	11 27 11.2	+17 01 48	Sbc	4.0	0.026	50.8	1.36	0.18	126.2	1131±39 ^c	12.15±0.11
NGC 3686	11 27 44.1	+17 13 26	SBbc	4.1	0.024	42.0	1.46	0.12	22.7	1096±36 ^c	11.84±0.07
NGC 3691	11 28 09.4	+16 55 14	SBb	3.0	0.026	47.4	1.17	0.15	22.0	1081±39 ^c	12.48±0.17
PGC 034537#	11 18 06.0	+18 47 53	Sc	4.9	0.023	23.3	0.73	0.04		1140±7	16.19±0.38
PGC 086629#	11 18 21.4	+17 41 51	I	9.8	0.021	0.0	0.89	0.00		1055±5	
UGC 06341#	11 20 00.7	+18 15 38	Sd	7.9	0.019	90.0	1.00	0.44	152.1	1611±42	15.96±0.39
PGC1534499#	11 21 25.41	+17 30 35.16	Sm	9.0	0.024	65.5	0.92	0.25	145.0	979±57	16.30±0.50
PGC 086673#	11 22 59.3	+17 28 27	I	10.0	0.021	0.0	0.79	0.00		1383±4	
PGC 035087#	11 25 01.8	+17 05 09	Sm	9.0	0.025					1208±5	
PGC035096#	11 25 10.8	+16 53 04	I	9.5	0.026	51.0	0.76	0.15	147.0	1021±3	15.96±1.17
PGC 035426#	11 29 54.4	+16 25 46	Im ^b		0.027					1067±5	

^adata from HYPERLEDA <http://leda.univ-lyon1.fr> (Paturel et al. 2003). ^b Taken from NED. ^c Taken from Ramella et al. (2002). ^d no value in HYPERLEDA and RC3. ^e Taken from RC3. ^f Taken from Petrosian et al. (2007). #Added members from Hyperleda. * SDSS galaxy misidentification.

and U376, since they map different regions within the Leo cloud (Tully 1988), in particular the associations 21-12+12 and 21-1+1, respectively. In addition to the UV and optical images, bright spirals of the two groups, were selected for a 2D kinematic study in order to map the galaxy velocity field and possible kinematical distortions.

In the catalog of Ramella et al. (2002), U268 is composed of 10 galaxies with $\langle V_h \rangle = 1454 \pm 67 \text{ km s}^{-1}$, apparent B magnitude of $\langle B_T \rangle = 14.26 \pm 0.98$ and $\sim 30\%$ of ETGs. U376 is composed of 16 galaxies with $\langle V_h \rangle = 1110 \pm 240 \text{ km s}^{-1}$, apparent B magnitude of $\langle B_T \rangle = 12.81 \pm 1.45$ and $\sim 50\%$ of ETGs.

We also include as new members of the two groups all

galaxies found in the HYPERLEDA database within the spatial and velocity extent defined by the catalog of Ramella et al. (2002). All galaxies in the HYPERLEDA database with velocity $\pm 3\sigma$ within the group average velocity given above and within a diameter of $\sim 1.5 \text{ Mpc}$ about the group center identified by Ramella et al. (2002) were included. All members thus chosen and their main characteristics are listed in Table 1. The table provides for each group, the name, the J2000 coordinates, the morphological type, the foreground galactic extinction, the inclination, the major axis diameter D_{25} , the axis ratio, the position angle (P.A.), the heliocentric systemic velocity and the B total apparent magnitude of the galaxy members. In Figure 1 (top panels), we show

the projected spatial distributions of the group members. Galaxies are separated in B magnitudes bins and for morphological types. ETGs, Spirals and Irregulars, with absolute magnitudes $M_B > -14$, $-18 < M_B < -14$ and, $M_B < -18$ are indicated with squares, triangles and circles of increasing size, respectively. In U376, the ETGs appear concentrate while the brightest Spirals form a substructure (see next section). On the contrary, U268 appears dominated by late type galaxies with only three S0s in the outskirts of the group. Dressler & Shectman (1988) ‘bubble-plots’ are also overlaid (see next subsection).

2.1 Substructure

The presence of substructure in a galaxy group is believed to be a signature of recent accretion and can be used as a probe of evolution of their members (e.g. Lacey & Cole 1993; Zabludoff & Mulchaey 1998a; Firth et al. 2006; Hou et al. 2012). Substructure manifests itself as a deviation in the spatial and/or velocity arrangement of the system.

If a galaxy group is a dynamically relaxed system, then the spatial distribution of galaxies should be approximately spherical and the velocity distribution a Gaussian. The presence of substructure indicates a departure from this quasi-equilibrium state. Substructure is indicated by at least one of the following characteristics: (1) significant multiple peaks in the galaxy position distribution, (2) significant departures from a single-Gaussian velocity distribution, and (3) correlated deviations from the global velocity and position distributions. The 1D (radial velocity histogram) and 2D (projected sky positions) tests could be questionable for galaxy groups, due to the relatively small number of galaxies members. The Anderson-Darling test, that Hou et al. (2009) report as a reliable tool to detect departures from Gaussian velocity distribution in small data sets, applied to the heliocentric radial velocity distributions of our two groups, does not significantly depart from normality.

The 3D tests use both velocity and spatial information to find substructures. Pinkey et al. 96 determined that the Dressler & Shectman (1988) test (DS test hereafter) is the most sensitive test for systems with as few as 30 members. Zabludoff & Mulchaey (1998b); Firth et al. (2006); Hou et al. (2012) show that the DS test is suitable to be applied to groups with a minor number of members. The DS test identifies a fixed number of nearest neighbors on the sky around each galaxy, computes the local mean velocity and velocity dispersion of the subsample, and compares these values with the average velocity and velocity dispersion of the entire group. The deviations of the local average velocity and the dispersion from the global ones are summed. In particular, for the galaxy i , the deviation of its projected neighbors is defined as $\delta_i = (\text{nn} + 1)/\sigma_{gr} [(v_{loc} - \bar{v})^2 + (\sigma_{loc} - \sigma)^2]$ where \bar{v} and σ^2 are the average velocity and the velocity dispersion of the entire group, v_{loc} and σ_{loc} are the local ones, and nn is the numbers of the nearest neighbour. The total deviation for the group is defined as the sum of the local deviations δ_i , $\Delta = \sum_i^N \delta_i$, where N is the number of the group members. If the group velocity distribution is close to Gaussian and the local variations are only random fluctuations, $\Delta \simeq N$, whereas $\Delta > N$ is an indication of probable substructure. To compute δ , we set the number of neighbors at $4 \approx N^{1/2}$ (see e.g. Silverman

Table 2. Results of the Dressler-Shectman substructure test.

Group	N_{gal}	Δ/N_{gal}	P-value
U268	21	1.37	0.037
U376	24	1.63	0.001

1986). Since δ_i are not statistically independent and velocity distribution could not be Gaussian even if there are no subgroups, it is necessary to test the reliability of the Δ statistic by comparing it with a Monte Carlo analysis. The velocities were randomly shuffled among the positions and the Δ was recomputed 10000 times producing the probability that the measured Δ is a random result. The significance of having substructure (the p-value) was quantified by the ratio of the number of the simulations in which the value of Δ is larger than the observed value, and the total number of simulations ($N(\Delta_{sim} > \Delta_{obs})/N_{sim}$). A small p-value, corresponds to a high significance of substructure detection. In the top panels of Figure 1, we also over plot the Dressler-Shectman ‘bubble-plots’ on each galaxy in the group as a circle whose radius scales with e_i^{δ} . Larger circles indicate larger deviations in the local kinematics compared to the global one. A local grouping of galaxies with similarly large circles may indicate a kinematically distinct system, i.e. a substructure. Both the groups present substructures, Δ is greater than N at a confidence level $> 95\%$ and $>99\%$ respectively (see Tab 2).

2.2 U268 and U376 environment

Are the large scale environments of the two groups in the Leo cloud similar? To investigate the environment of each group we considered the galaxy distribution within a box of 4 Mpc, about two times the size of a typical group, centred on the brightest galaxy **in B band** of each group (NGC 3003 and NGC 3067 in U268 and U376, respectively). From the HYPERLEDA database we select galaxies with a heliocentric radial velocity within $\pm 3\sigma$ of the group mean velocity given in the catalog of Ramella et al. (2002) finding 64 and 268 galaxies in U268 and U376 box, respectively (+ symbols in Figure 1, bottom panels, see also Appendix B). In the middle panels of Figure 1 we highlights (filled bins) the velocity distribution of group members given in Table 1 superposed to the distribution of the heliocentric radial velocity, in the range 10 and 3000 kms^{-1} , of galaxies in the box of 4 Mpc.

Among these galaxies, to mark the ‘bone’ of the galaxy groups, we selected only galaxies more luminous than 15.5 B-mag, i.e the magnitude limit of the galaxies in Ramella et al. (2002). On this sample we performed a density analysis. The 2D binned kernel-smoothed number contours maps are shown in the bottom panels of Figure 1). Density in the box is colour coded. The highest densities correspond to the red regions; density levels above 0.005 are in yellow. Blue squares show the members of the two groups in the catalog of Ramella et al. (2002), green diamonds indicate the new members we added as explained in section 2.1.

Density contour maps show that galaxy members of U268 and U376 are, in projection, part of elongated structures, revealing sub-structures, as found in the previous section. The quite large separation of ~ 1.6 Mpc among the members, suggests that U268 is a very loose configuration,

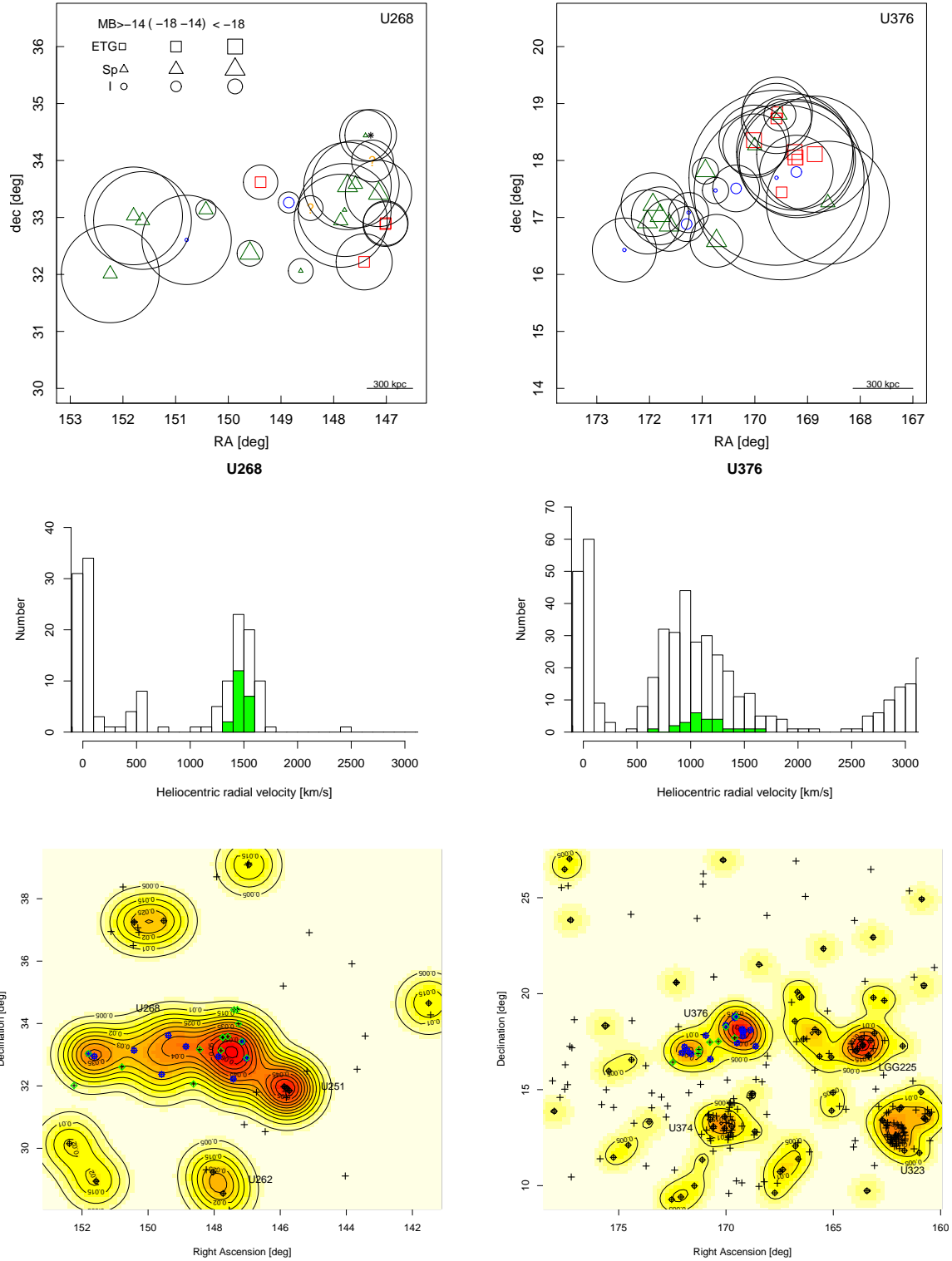


Figure 1. (*Top panels*) Spatial distribution of galaxies we consider as group members. Galaxies are separated in B magnitude bins and for morphological type. Unknown morphological types with known B magnitudes are labelled with "?". The smallest symbols are galaxies with no B magnitudes. Black asterisks refer to galaxies with no B magnitudes and no morphological types. Dressler & Shectman (1988) 'bubble-plots' are also overlaid. (*Middle panels*) Histogram of heliocentric radial velocity in the range 10-3000 kms^{-1} of galaxies within a box of 4 Mpc centred on the respective B brightest member of the two groups. The width of the velocity bins is 100 kms^{-1} . Green bins show the velocity extent of the members of the two groups. (*Bottom panels*) Spatial distribution of galaxies (**black plus**) within the velocity extent defined by the members in the catalog of Ramella et al. (2002). The two squares are centred on NGC 3003 and NGC 3067 in U268 and U376 respectively. Blue square symbols show the members of the two groups listed in the catalog of Ramella et al. (2002), green diamond ones indicate the added members. The 2D binned kernel-smoothed number density contours for the galaxies with $m_B \leq 15.5$ (circle + cross) are also shown.

at the borderline with the field. In U268 the two substructure, identified in the previous section, appear also likely connected to another structure which includes USGC U251 detect by Ramella et al. (2002) as a single group.

Galaxy members of U376 have a more **patchy** configuration than U268. The environment appears rich of galaxies and crowded by tight associations. Several other galaxy groups (USGC U323 and USGC U374), including LGG 225, already analysed in Paper I, have been identified in the nearby surroundings of U376 (Figure 1, bottom right panel).

3 OBSERVATIONS AND DATA REDUCTION

3.1 UV and optical data

The UV imaging was obtained from *GALEX* (Martin et al. 2005; Morrissey et al. 2007) GI6-6017 (PI A. Marino) and archival data in two ultraviolet bands, far-UV (FUV, 1344 – 1786Å) and near-UV (NUV, 1771 – 2831Å). The instrument has a very wide field of view ($1^\circ.25$ diameter) and a spatial resolution of $\approx 4''.2$ and $5''.3$ FWHM in FUV and NUV respectively, sampled with $1''.5 \times 1''.5$ pixels (Morrissey et al. 2007).

The exposure times (see Table 3) for most of our sample are ~ 100 sec (limiting AB magnitude in FUV/NUV of $\sim 19.9/20.8$ (Bianchi 2009)). NGC 3011 in U268 and a few galaxies in U376 have an exposure time ~ 10 times longer (~ 2.5 AB mag fainter limit). We used FUV and NUV intensity images to compute integrated photometry of the galaxies and light profiles, as described in Sect. 4.1.

In addition, we used optical Sloan Digital Sky Survey (SDSS) archival data in the u [2980-4130 Å], g [3630-5830 Å], r [5380-7230 Å], i [6430-8630 Å], z [7730-11230 Å] filters (Adelman-McCarthy et al. 2008).

Figure 2 and Figure 3 display colour composite UV (FUV blue, NUV yellow, left panels) and optical (SDSS, g blue, r green, i red) images of the galaxy members of U268 and U376 respectively as listed in the catalog of Ramella et al. (2002). All UV and optical colour composite images of the added galaxy members but PGC 2016633 are shown in Appendix A.

3.2 2D kinematical observations and data reduction of a subset of spirals

Observations were done in 2011 February, at the Cassegrain focus of the 2.12m telescope at the Observatorio Astronómico Nacional in San Pedro Mártir (México), using the scanning Fabry - Perot interferometer² PUMA (Rosado et al. 1995). PUMA instrument uses a Thomson2k 2048x2048 pixels CCD detector with a pixel size of $15 \times 15 \mu$. The readout noise was $5.7e^-$. A 1500×1500 px window has been used, and a 3×3 binning performed, giving an pixel equivalent to $1.07''$ on the sky. Table 4 provides the journal observations and the characteristics of the interferometer we used.

² All Fabry - Perot data (cubes, moment maps and rotation curves) are available at [FabryPerot.oamp.fr](http://www.fabryperot.oamp.fr), in the loose group survey

Table 3. Journal of the *GALEX* observations.

Group Galaxies	FUV Exp. Time [sec]	NUV Exp. Time [sec]
U268		
MRK 0408	186	186
NGC 3003	186	2579
NGC 3011	1543.05	1688
UGC 05287	206	1533
UGC 05326	278	278
IC 2524	278	1626
NGC 3067	200	1884
UGC 05393	109	1643
UGC 05446	112	1661
NGC 3118	112	1884
PGC 2016633	186	186
PGC 2042146	192	192
SDSS J094911.28+342634.2	192	192
SDSS J094935.09+342616.3	192	192
NGC 3021	206	206
UGC 05282	206	1533
PGC 2025214	206	1533
SDSS J095430.02+320342.0	199	420
SDSS J100309.92+323622.5	109	109
U376		
NGC 3592	3715	3715
NGC 3599	2468.05	2468.05
NGC 3605	2468.05	2468.05
UGC 06296	2468.05	2468.05
NGC 3607	2468.05	2468.05
NGC 3608	2468.05	2468.05
CGCG 096-024	135	1658
UGC 06320	90	90
UGC 06324	90	90
NGC 3626 ¹		
NGC 3655	106.1	106.1
NGC 3659 ¹		
NGC 3681	106.1	106.1
NGC 3684	107.05	107.05
NGC 3686	105	105
NGC 3691	107.05	107.05
PGC 034537	93	93
PGC 086629	135	135
PGC 035087	112	112
PGC 035096	112	112
PGC 035426	110	110

¹ No *GALEX* observations for these galaxies. **Unfortunately the *GALEX* observations of the two galaxies, awarded as part of the GI6-6017 proposal, have not been completed.**

3.2.1 Moment maps

PUMA data have been reduced using the ADHOCw software procedures of Boulesteix³, and Daigle et al. (2006)⁴. The first step, before the correction phase, was to perform the standard CCD data reduction by applying bias and flat field corrections. The data reduction procedure has been extensively described in Amram et al. (1996); Daigle et al. (2006); Epinat et al. (2008a), Epinat et al. (2008b). Wavelength calibration was obtained by scanning the narrow NeI 6599Å line under the same observing conditions. Velocities measured relative to the systemic velocity are very accurate, with an error of a fraction of a channel width (< 3 km s⁻¹) over the whole field. The signal measured along the scanning sequence was separated into two parts: (1) an almost constant level produced by the continuum light in

³ Available at <http://www.oamp.fr/adhoc/distribution/>

⁴ Available at <http://www.astro.umontreal.ca/odaigle/reduction/>

Table 4. Journal of H α observations

	NGC3659 / NGC3684 / NGC3691 / UGC05287	NGC3655 / NGC3686 / UGC05393
Observations		
Telescope	OAN 2.1m	OAN2.1m
Date	Feb. 2 nd 2011	Feb. 4 th 2011
Instrument	PUMA	PUMA
Interference Filter		
Central Wavelength (Å)	6607	6607
FWHM (Å)	89	89
Transmission (%) @ V_{sysFP}	65 / 66 / 67 / 63	67 / 66 / 63
Calibration		
Neon Calib. Lamp (Å)	6598.95	6598.95
Perot-Fabry		
Interference Order	330@H α	330@H α
Free Spectral Range	910km.s ⁻¹	910km.s ⁻¹
Finesse@H α	24	24
Spec. Resolution@H α	8000	8000
Sampling		
N. of Channels	48	48
Sampling step (Å)	0.43	0.43
equivalent (km.s ⁻¹)	19	19
Pixel Size	1.07''	1.07''
Detector		
	Thomson 2k	Thomson 2k
Exposure Time		
Total exp. (h)	1.6	3.2
Eleme. exp./chan (s)	120	120

a 15 Å passband around H α (continuum map), and (2) a varying part produced by the H α line (H α integrated flux map). The continuum is computed by taking the mean signal outside the emission line. The H α integrated flux map was obtained by integrating the monochromatic profile in each pixel. The velocity sampling was 19 km s⁻¹. Strong OH night sky lines passing through the filters were subtracted by determining the level of emission away from the galaxies (Laval et al. 1987). In order to improve the S/N ratio, we used the adaptive smoothing (Voronoi **tessellation**) as described in Daigle et al. (2006, and references within). The different maps presented in this paper has been made adopting a final SNR of 5 or 6, depending of the galaxies. In any case, a rectangular smoothing of 3 channels have been also applied.

Figures 4 and 5 show the monochromatic H α maps, the 2D velocity maps and the dispersion velocity maps of spirals, in U268 and U376, respectively.

3.2.2 Rotation Curves

Figure 6 shows the H α rotation curves (RCs) of UGC 05287 in U268 and NGC 3655, NGC 3659, NGC 3684, NGC 3686, NGC 3691 in U376.

Epinat et al. (2008b) provide the details about the method used to derive the RCs. The fitting method is similar to that adopted by Barnes & Sellwood (2003), the main difference being in the determination of the velocity uncertainties. The adopted technique takes into account errors

due to non circular motions (e.g. presence of a bar, spiral arms, etc.). The code fits different parameters of the modeled velocities in polar coordinates for different bins or crowns (Epinat et al. 2008b, their Appendix A). The input parameters, coordinates of the centre (x_c , y_c), systemic velocity (v_{sys}), position angle (PA) and galaxy inclination (i) are taken from the literature in order to constrain the fit. Table 6 summarises the kinematical results. Inclination and position angles are derived from both velocity and continuum maps.

4 RESULTS

4.1 Photometry and surface brightness profiles

The UV and optical surface photometry was carried out using the ELLIPSE fitting routine in the STSDAS package of IRAF (Jedrzejewski 1987). The SDSS images (corrected frames with the soft bias of 1000 counts subtracted) in the five bands were registered to the corresponding GALEX NUV intensity images before to evaluate brightness profiles, using the IRAF tool `register`. We masked the foreground stars and the background galaxies in the regions where we measured the surface brightness profiles. **To secure a reliable background measure, we force the measure of 5 isophotes well beyond the galaxy emission.**

From the surface brightness profiles, we derived total apparent magnitudes as follows. For each profile, we computed the integrated apparent magnitude within elliptical

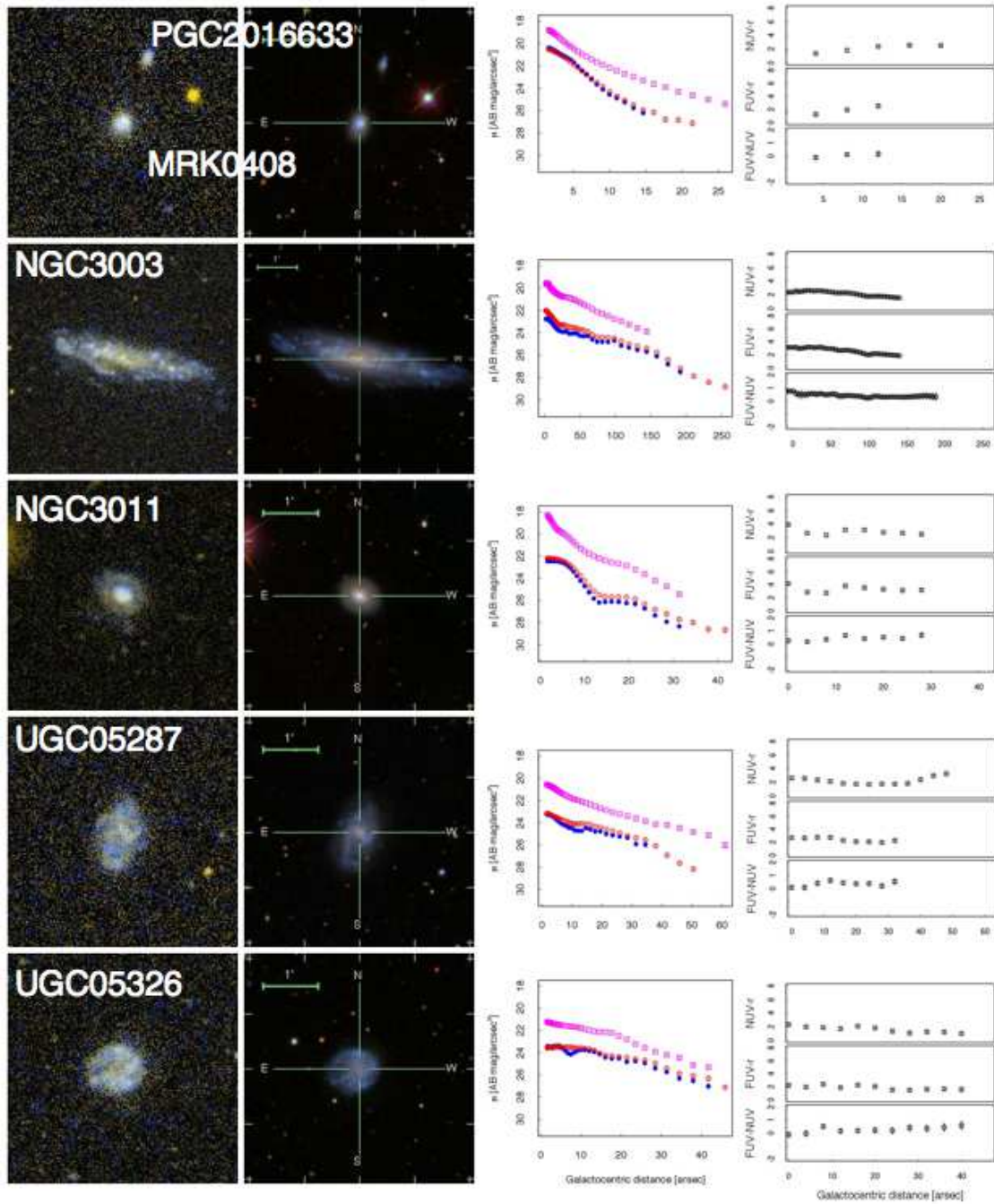


Figure 2. From left to right: colour composite UV (FUV blue, NUV yellow) and optical (SDSS, g blue, r green, i red) images of 5 members of U268; UV (FUV blue, NUV red) and optical (SDSS- r magenta) surface luminosity, and colour profiles, corrected by galactic extinction.

isophotes up to the radius where the mean isophotal intensity is 2σ above the background. The background was computed around each source, as the mean of sky value of the outer five isophotes. Errors of the UV and optical magnitudes were estimated by propagating the statistical errors on the mean isophotal intensity provided by ELLIPSE. In addition to the statistical error, we added an uncertainty to account for systematic uncertainties in the zero-point calibration of 0.05 and 0.03 mag in FUV and NUV respectively (Morrissey et al. 2007). Surface photometry was cor-

rected for galactic extinction assuming Milky Way dust with $R_v=3.1$ (Cardelli et al. 1989), $A_{FUV}/E(B-V) = 8.376$ and $A_{NUV}/E(B-V) = 8.741$, $A_r/E(B-V) = 2.751$.

Figure 2 and Figure 3 display brightness and colour profiles of bright members of the 2 groups. Table 5 lists the measured foreground extinction uncorrected AB magnitudes both in UV and optical⁵ bands. We used UV and

⁵ We converted SDSS counts to magnitudes following the recipe provided in

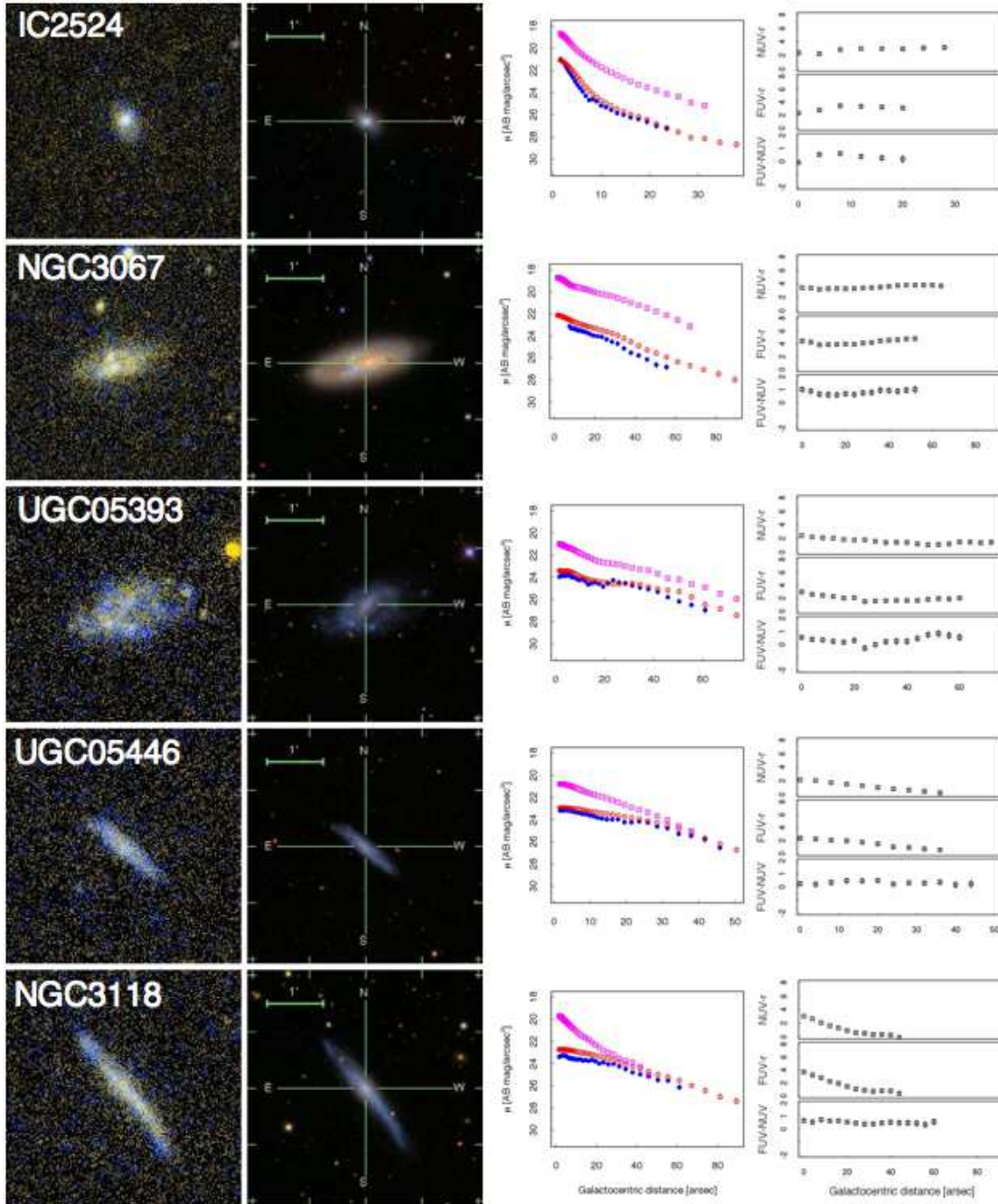


Figure 2. Continued.

optical images and luminosity profiles to obtain a more robust morphological classification, we also report in Table 5. UV and optical magnitudes of fainter added members were extracted from the *GALEX* and SDSS pipelines. We used the FUV and NUV calibrated magnitudes and the Model magnitudes⁶ from the *GALEX* and SDSS pipelines, respectively.

<http://www.sdss.org/df7/algorithms/fluxcal.html>
#counts2mag.

⁶ <http://www.sdss.org/dr5/algorithms/photometry.html>

In the next two sections we describe the morphology, the luminosity and the colour profiles of individual galaxies. The main purpose is to identify peculiarities possibly associated to interaction events.

4.1.1 *U268: individual morphological and photometric notes*

The group is composed of a large fraction of late-type galaxies.

MRK 408 The galaxy is nucleated both in UV and optical images. Its outer isophotes appear elongated toward

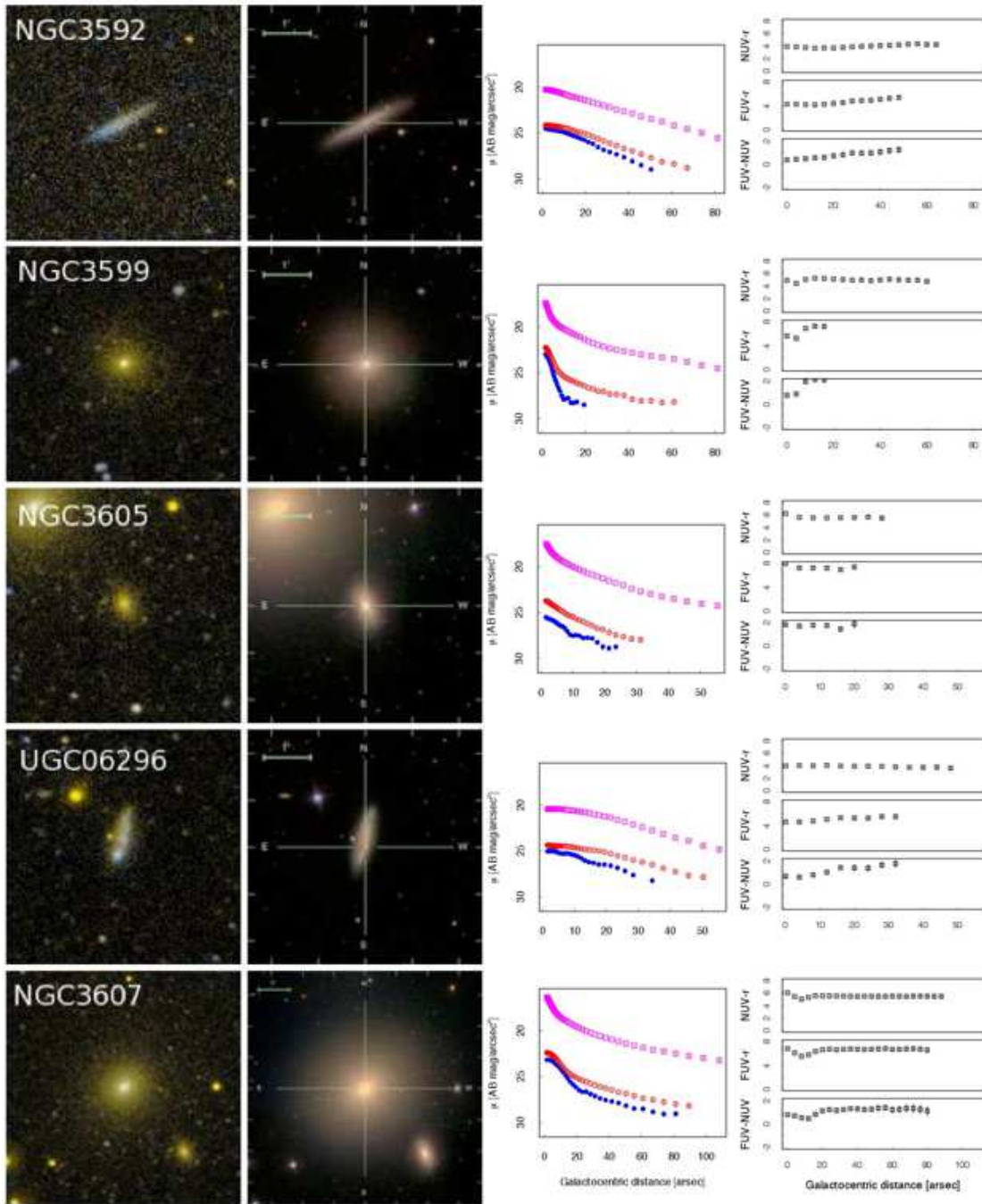


Figure 3. As in Figure 2 for U376 galaxy members.

the SE. Neither arms, nor fluculent structures are visible. The UV and optical luminosity profiles may be decomposed into a bulge+disk component so that the galaxy is a S0. The galaxy is blue ($FUV - NUV \approx 0$) along its extension.

NGC 3003 The galaxy is a nearly edge-on spiral. Its SW and NE parts are asymmetric, and signatures of perturbation are likely present in this latter part. In the southern part, the UV composite image shows distorted arm/tails not revealed in the optical image. Luminosity profiles are typical of a spiral galaxy. The outer disk is bluer than the nuclear part ($FUV - NUV \approx 0$ vs. $FUV - NUV \approx 0.7$). The r pro-

file is truncated since the image is at the edge of the FOV and does not allow an accurate surface photometry.

NGC 3011 In this S0 galaxy, the presence of an outer ring is visible in the UV. The r luminosity profile shows the presence of two components, the bulge and the disk (emerging at $\approx 20''$). The ring shows a blue ($FUV - NUV = 0.3$) colour as those presented in Marino et al. (2011).

UGC 5287 Galaxy is a nearly face-on spiral with open arms starting from a bar. The Northern and the Southern arms appear asymmetric in the optical image. At the end of the southern arm, in the NUV image is well visible a bright region that could be a possible dwarf companion.

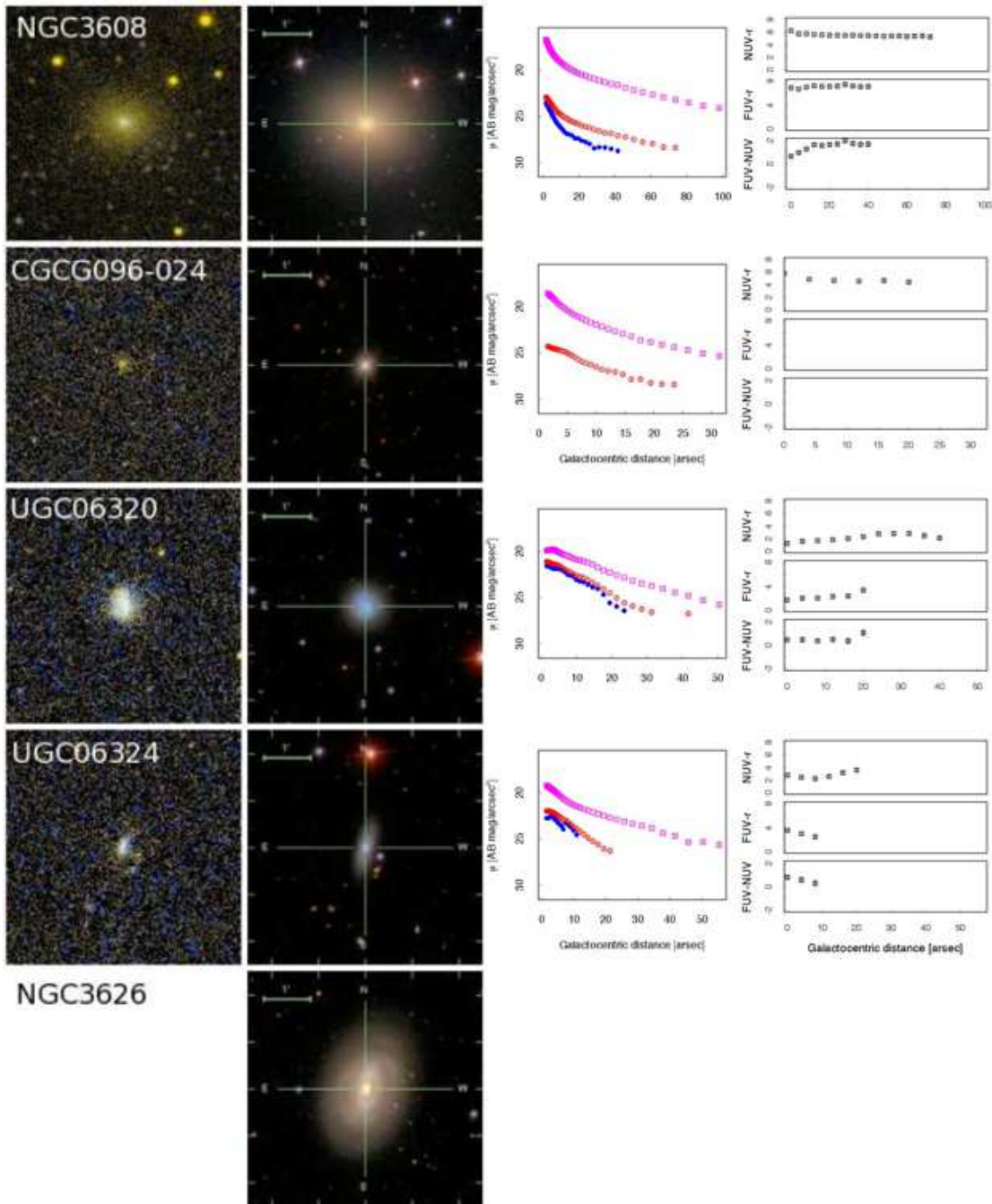


Figure 3. Continued.

UGC 5326 This spiral is reminiscent of the Cartwheel. The nucleus is displaced in the NW direction with respect to the centre of the outer ring. All the galaxy is blue in the UV ($FUV - NUV \approx 0$), while in the more resolved optical images, the ring is bluer than the nucleus ($FUV - r$ and $NUV - r \approx 1$). Deeper higher resolution images are needed to clarify the nature of this galaxy.

IC 2524 The major axis of the UV and optical images of the galaxy, likely an S0, are different. The P.A. of the optical isophotes is about 45° NE at odds with UV isophotes having a P.A. $\approx 10^\circ$ NE. The galaxy is quite blue for its mor-

phological class especially in the outskirts ($FUV - NUV = 0$). Outer isophotes seem boxy.

NGC 3067 The UV and optical images indicate that this is a disk galaxy. It is classified as a spiral in HYPERLEDA: our images do not show unambiguous arms. Blue spots ($FUV - NUV \approx 0.5$) are detected in the inner SE part. The nuclear part is red ($NUV - r \approx 3.9$) and a dust system is likely present.

UGC 5393 The UV image is more extended than the optical one. In this latter the arms appear to start from a bar and close forming a ring. Signatures of interaction (tail)

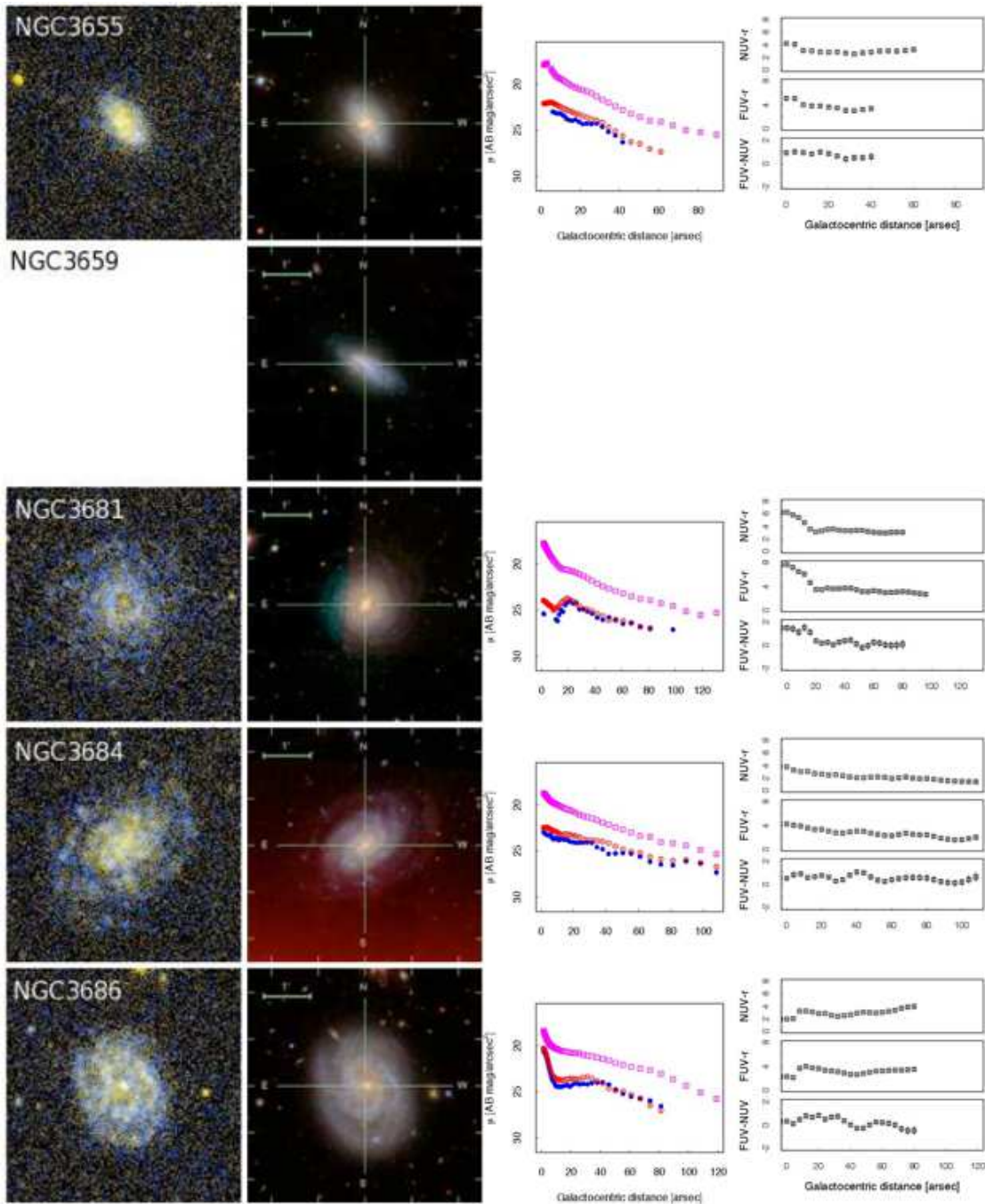


Figure 3. Continued.

are present in the SE. A blue ring ($FUV - NUV \approx 0$) is visible in the both UV luminosity colour profiles.

UGC 5446 The galaxy is seen edge-on. We suspect a warp in the NE side of the galaxy. UV and optical surface photometry do not show evidence of a nucleus. The galaxy outskirts are bluer than the inner parts ($FUV - r \approx 2$; $NUV - r \approx 2$, and ≈ 0) in the centre.

NGC 3118 The galaxy is seen edge-on showing unambiguous warps. The luminosity and colour profiles show a red bulge ($FUV - r \approx 4$) and a quite blue disk ($FUV - r$ and $FUV - NUV \approx 0$).

4.1.2 *U376: individual morphological and photometric notes*

NGC 3592 The galaxy is seen edge-on with a dust lane along the major axis. The luminosity profiles suggest that it is basically composed of a disk which is quite red ($FUV - NUV \approx 1$) compared with edge-on galaxies described in this paper. No signature of interaction.

NGC 3599 This S0 galaxy does not show signature of interaction. The FUV emission has a very limited extension. The galaxy is quite red ($FUV - NUV$ between 1 and 2; $FUV - r \approx 6$; $NUV - r \approx 5$).

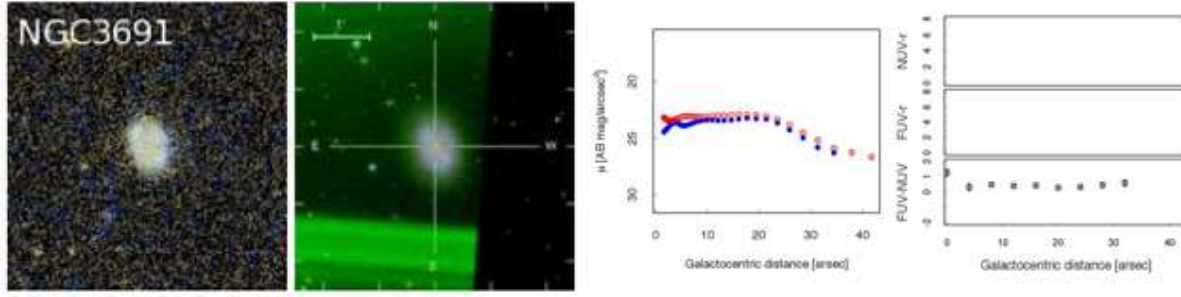


Figure 3. Continued.

Table 5. UV and optical photometry. Column 2 also reports our morphological type classification.

Group galaxy	Type	FUV [AB mag]	NUV [AB mag]	u [AB mag]	g [AB mag]	r [AB mag]	i [AB mag]	z [AB mag]
U268								
MRK 0408	S0	16.126±0.062	15.896±0.047	15.368±0.041	14.602±0.024	14.263±0.024	14.123±0.035	14.044±0.049
NGC 3003	Sbc	14.233±0.079	13.835±0.040	13.371±0.083	12.654±0.076	12.081±0.062	11.933±0.055	11.666±0.063
NGC 3011	S0(R)	16.824±0.064	16.502±0.046	15.433±0.071	14.118±0.021	13.539±0.020	13.229±0.029	13.040±0.036
UGC 05287	SBc	16.272±0.092	15.903±0.045	15.199±0.158	14.051±0.042	13.737±0.041	13.541±0.067	13.433±0.103
UGC 05326	Sc(R)pec	15.767±0.115	15.589±0.058	14.926±0.121	14.099±0.031	13.823±0.037	13.647±0.055	13.646±0.082
IC 2524	S0	16.748±0.075	16.385±0.043	15.636±0.070	14.599±0.025	14.227±0.029	14.063±0.033	13.963±0.053
NGC 3067	Sappec	16.367±0.095	15.556±0.050	13.838±0.066	12.597±0.054	11.935±0.051	11.563±0.052	11.330±0.045
UGC 05393	SBb	15.691±0.093	15.534±0.050	14.780±0.149	14.015±0.048	13.789±0.043	13.709±0.057	13.789±0.110
UGC 05446	Sc	16.717±0.090	16.380±0.056	15.777±0.102	14.966±0.053	14.656±0.034	14.482±0.043	14.522±0.103
NGC 3118	Sbc	16.086±0.102	15.594±0.054	14.766±0.094	13.867±0.042	13.591±0.036	13.343±0.041	13.370±0.089
PGC2016633	S0?	18.100±0.060	17.922±0.035	17.728±0.020	16.824±0.004	16.511±0.004	16.399±0.004	16.311±0.016
PGC2042146	?	18.247±0.059	18.203±0.041	17.767±0.023	17.054±0.005	16.885±0.006	16.868±0.006	16.826±0.033
SDSSJ094911.28+342634.2	?	18.300±0.057	18.180±0.038	17.792±0.015	17.186±0.005	17.080±0.005	17.056±0.005	17.006±0.020
SDSSJ094935.09+342616.3	Sd	16.731±0.028	16.602±0.019	15.510±0.020	15.650±0.010	15.270±0.010	15.340±0.010	15.290±0.020
PGC082546	Sc			17.348±0.013	16.474±0.004	16.142±0.004	16.022±0.004	15.890±0.013
NGC3021	Sbc	15.394±0.017	14.831±0.008	14.120±0.003	12.838±0.002	12.255±0.002	11.820±0.002	11.556±0.002
UGC05282	Sm	17.488±0.046	17.126±0.024	16.630±0.030	15.550±0.010	15.170±0.010	15.370±0.010	14.940±0.020
PGC2025214	?	18.512±0.066	18.457±0.045	18.413±0.047	17.740±0.010	17.446±0.011	17.410±0.011	17.161±0.044
SDSSJ095430.02+320342.0	Sd	19.729±0.112	19.615±0.059	19.101±0.089	18.103±0.024	17.730±0.023	17.675±0.023	17.431±0.065
SDSSJ100309.92+323622.5	Irr	18.982±0.116	18.541±0.071	17.935±0.059	17.228±0.035	16.503±0.015	16.372±0.015	16.470±0.071
PGC029522	S0?			17.302±0.016	16.383±0.004	16.013±0.004	15.849±0.004	15.664±0.012
U376								
NGC 3592	Sd	17.924±0.064	17.285±0.061	15.586±0.102	14.090±0.037	13.466±0.034	13.122±0.044	12.959±0.064
NGC 3599	S0	18.670±0.092	17.045±0.089	14.314±0.099	12.585±0.049	11.911±0.043	11.569±0.042	11.408±0.042
NGC 3605	E	19.979±0.179	18.165±0.081	15.003±0.065	13.092±0.029	12.401±0.030	11.993±0.029	11.810±0.037
UGC 06296	Sc	18.573±0.084	17.767±0.064	15.786±0.118	14.358±0.035	13.698±0.033	13.300±0.032	13.042±0.050
NGC 3607	S0	16.954±0.087	15.683±0.067	12.723±0.062	10.742±0.044	9.974±0.041	9.534±0.042	9.301±0.037
NGC 3608	E	18.063±0.132	16.598±0.076	13.505±0.063	11.539±0.034	10.807±0.032	10.405±0.033	10.149±0.037
CGCG 096-024	S0		18.829±0.097	16.144±0.083	14.481±0.046	13.914±0.025	13.516±0.041	13.466±0.071
UGC 06320	S0?	15.722±0.087	15.268±0.054	14.388±0.050	13.607±0.029	13.208±0.027	13.026±0.032	12.954±0.066
UGC 06324	S0	17.707±0.098	17.071±0.078	15.831±0.075	14.391±0.032	13.915±0.038	13.688±0.050	13.574±0.063
NGC 3626	SB0r(R)							
NGC 3655	Sb	15.512±0.087	14.766±0.047	13.336±0.039	12.113±0.024	11.523±0.023	11.252±0.023	11.058±0.036
NGC 3659	SBd							
NGC 3681	SAB(r)bc	15.235±0.119	14.909±0.092	13.592±0.097	12.274±0.024	11.617±0.026	11.260±0.028	11.112±0.052
NGC 3684	SAB(r)bc	14.653±0.089	14.244±0.067	13.245±0.082	12.141±0.028	11.676±0.027	11.640±0.039	11.261±0.060
NGC 3686	SB(s)bc	14.414±0.073	13.895±0.052	12.847±0.059	11.614±0.022	11.079±0.021	10.784±0.020	10.633±0.050
NGC 3691	SBb	15.608±0.051	15.165±0.030					
PGC034537	SB(r)bc	18.319±0.095	17.950±0.054	17.614±0.028	16.225±0.004	15.607±0.003	15.235±0.003	15.000±0.007
PGC086629	Irr	19.351±0.128	18.667±0.087	21.915±0.376	21.409±0.099	20.746±0.085	20.256±0.085	21.476±0.793
UGC06341	Sd			16.915±0.020	15.709±0.005	15.391±0.004	15.235±0.004	15.192±0.016
PGC1534499	S0?			17.564±0.041	16.108±0.005	15.475±0.005	15.111±0.005	15.184±0.032
PGC086673	Irr			18.271±0.082	17.637±0.055	16.822±0.027	16.643±0.027	16.549±0.067
PGC035087	Irr?	19.624±0.167	19.534±0.132	17.946±0.086	16.961±0.012	16.559±0.013	16.465±0.013	16.318±0.081
PGC035096	Irr	18.254±0.081	17.972±0.056	21.977±0.230	22.937±0.196	22.871±0.266	23.533±0.266	22.083±0.659
PGC035426	Im	20.210±0.205	19.729±0.127	18.598±0.108	17.306±0.012	16.811±0.018	16.665±0.018	16.603±0.058

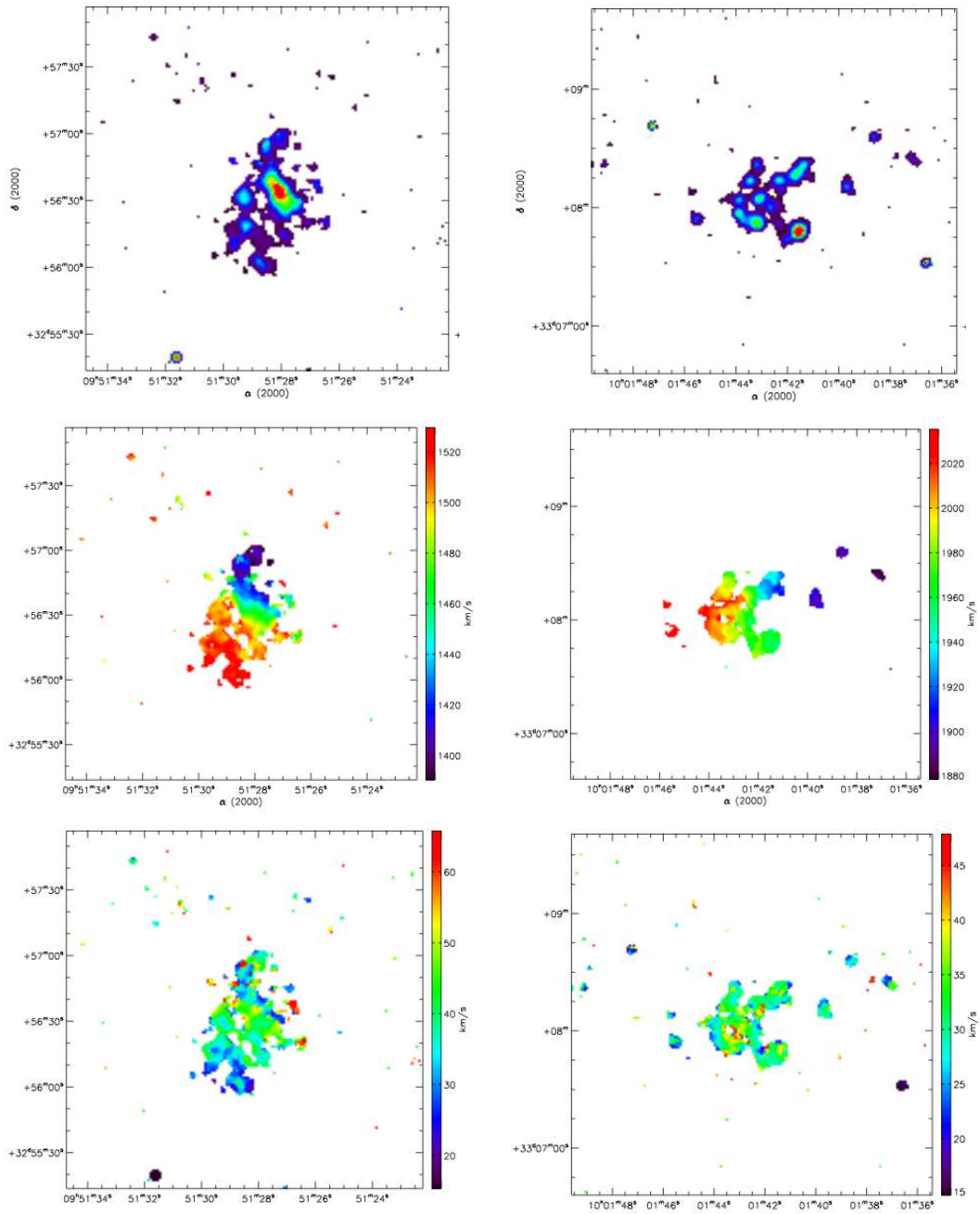


Figure 4. From top to bottom: monochromatic H α image, velocity field and ionized gas velocity dispersion of UGC 05287 (left panels) and UGC 05393 (right panels) in U268.

NGC 3605 We found indication of outer shells, likely due to a past accretion event (Dupraz & Combes 1986) or a weak interaction (Thomson 1991). The galaxy luminosity profile is typical of an elliptical. Far UV and optical colours are red ($FUV - NUV \approx 1.5$; $FUV - r \approx 7$; $NUV - r \approx 5$).

UGC 6296 This is a disk galaxy, not an Irregular as in the classification of Table 1 from HYPERLEDA. Both the UV and the optical images suggest the presence of dust absorption features. It is reminiscent of NGC 3067 in U268. In the SE part, a blue knot is detected in the UV images ($FUV - NUV \approx 0.3$).

NGC 3607 This bright elliptical does not show sig-

nature of interaction. The galaxy is red as shown by the UV and optical luminosity and colour profiles. Average colours are: $FUV - NUV \approx 1$; $FUV - r \approx 6$; $NUV - r \approx 5.9$.

NGC 3608 No signature of interaction in this red-and-dead elliptical galaxy (Rampazzo et al. 2012 in prep.).

CGCG 096-024 Faint nucleated galaxy undetected in FUV, likely an elliptical as suggested by the optical profile. The galaxy is red ($NUV - r \approx 5$).

UGC 6320 A blue ($FUV - NUV \approx 0.5$; $FUV - r \approx 2$; $NUV - r \approx 2$), face-on disk galaxy, apparently without a bulge. A blue polar ring is visible in the optical image. UV images are faint due to the low exposure time.

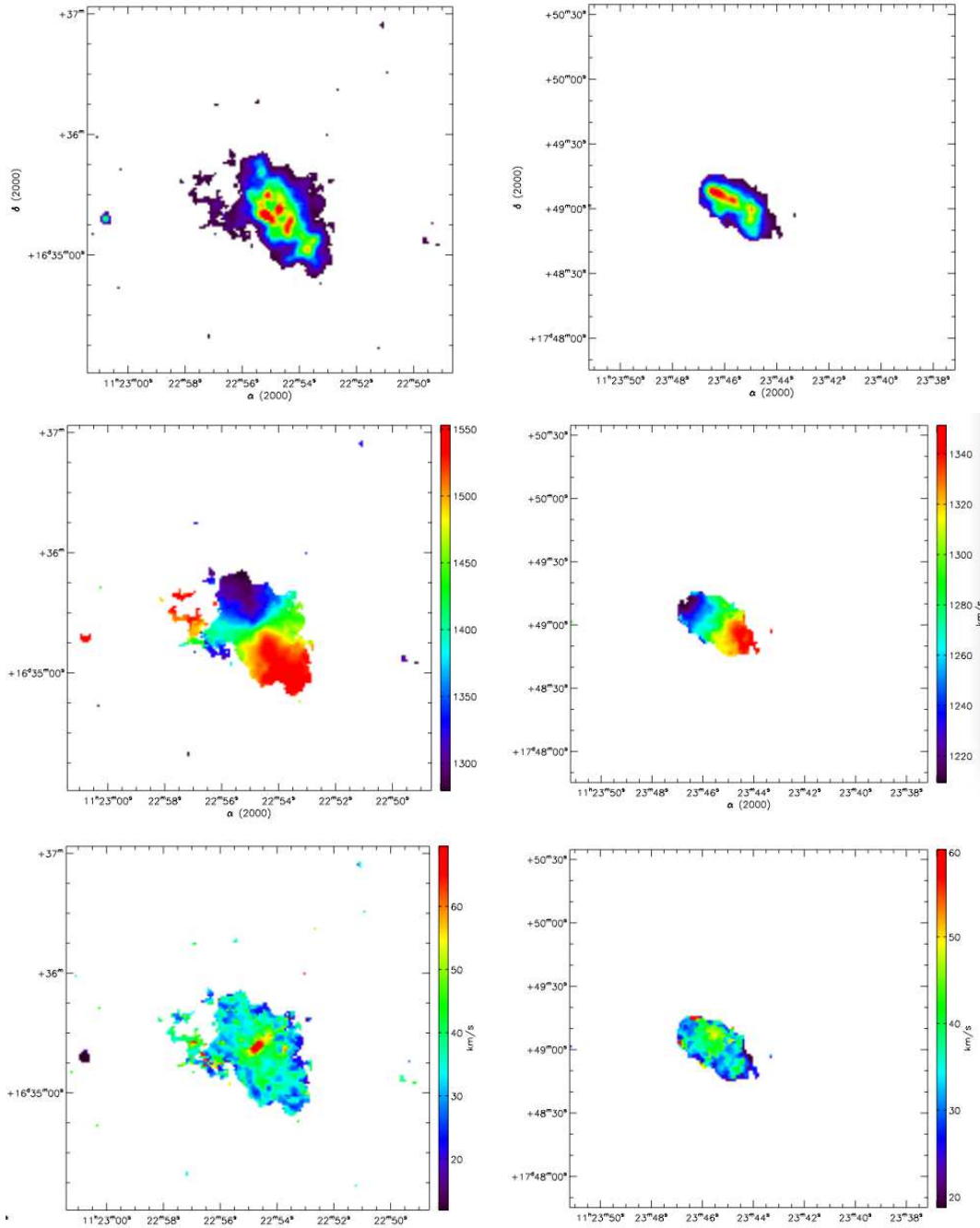


Figure 5. As in Figure 4 for NGC 3655 (left panels) and NGC 3659 (right panels) in U376.

UGC 6324 Nucleated disk galaxy, likely an S0 as classified in Table 1. No interaction signatures are visible. The luminous objects in the SW of the nucleus are a foreground star and a background galaxy as can be seen in the SDSS composite image.

NGC 3626 Barred S0 galaxy with inner and outer ring structures. No UV images are available for this galaxy.

NGC 3655 Classified as Sb in HYPERLEDA, the galaxy shows a red dusty bulge ($FUV - NUV \approx 1$; $FUV - r \approx 5$; $NUV - r \approx 4$) and a blue ($FUV - NUV \approx 0.5$; $FUV - r \approx 3$; $NUV - r \approx 2.1$) disk. The faint outer arms may be generated by interaction (see UV image). The galaxy in

the SDSS composite image shows a possible polar ring-like structure.

NGC 3659 Barred spiral with regular arms seen at high inclination. UV observations are lacking.

NGC 3681 Face-on spiral galaxy. Arms appear wrapped up. The far-UV image is much more extended than the optical one and arms have a flocculent aspect. No signature of interaction. The UV image and the surface photometry reveal evidence of an inner ring which can be guessed also in the optical. The ring may be connected with the presence of a bar structure visible only in the optical bands. The

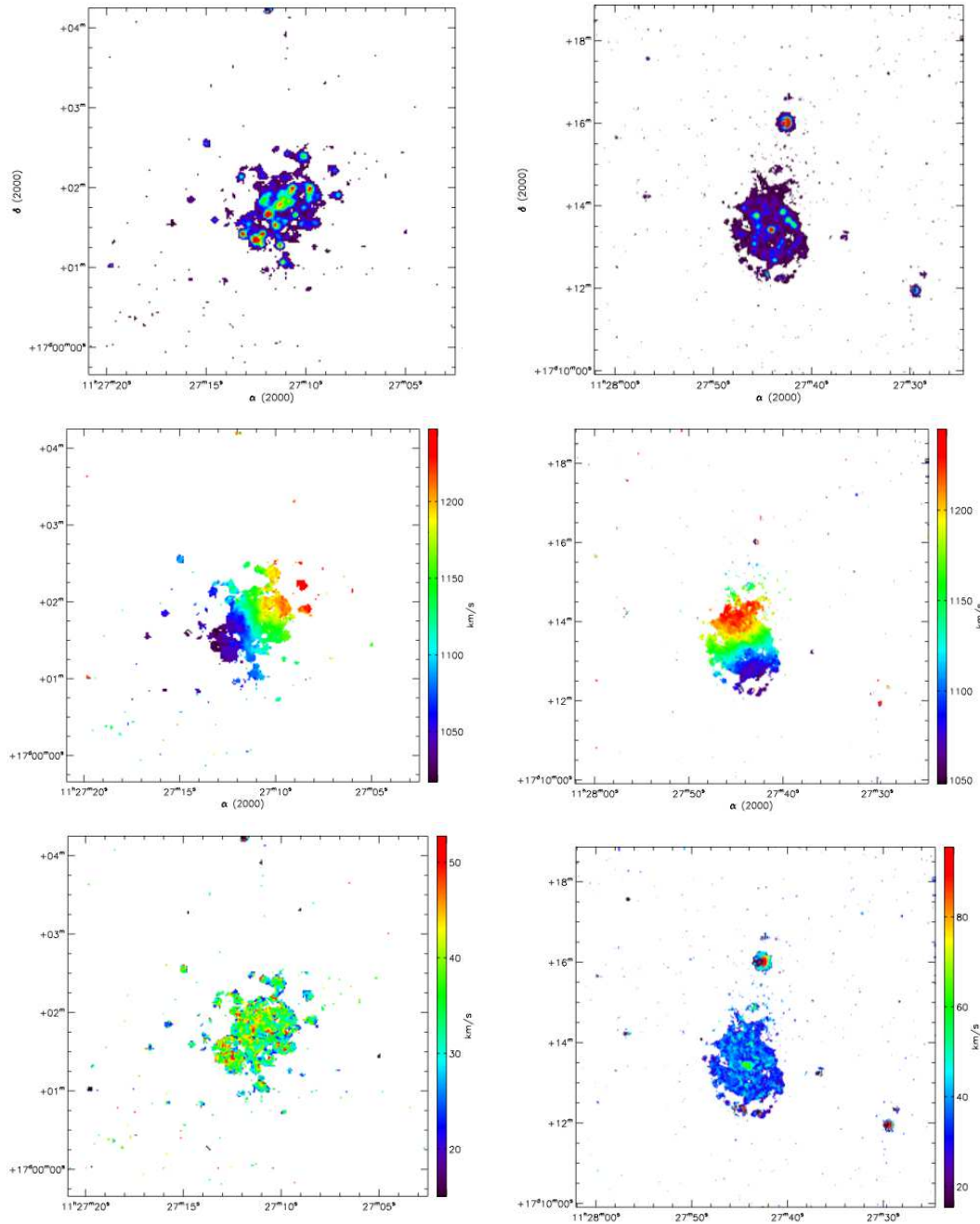


Figure 5. As in Figure 4 for NGC 3684 (left panels) and NGC 3686 (right panels) in U376.

colours of the ring are $FUV - NUV \approx 0$; $FUV - r \approx 4$; $NUV - r \approx 3.8$.

NGC 3684 Spiral galaxy. The UV image is more extended than the optical one. No unambiguous signature of interaction.

NGC 3686 Spiral galaxy seen nearly edge-on. The bar is barely visible. No obvious signature of interaction. UV and UV-optical colours are typical of spirals (see figures 9 and 10 in Marino et al. (2010), and figure 4 in Marino et al. (2011)).

NGC 3691 Disk galaxy. The bar is barely visible as well as arms in the blue disk. The quality of the optical images do not allow photometric measures.

4.2 Description of the kinematics of the spiral galaxies

4.2.1 U268: individual kinematics notes

We obtained kinematical data for two spiral galaxies in U268, namely UGC 05287 and UGC 05393.

UGC 05287 The signature of the bar is present in the velocity field which is irregular and highly asymmetric. The blue-shifted side of the velocity field is almost inexistent. In the r -SDSS and UV images, the morphology of the galaxy is very asymmetric. Beside the bar, the galaxy exhibits a large spiral arms towards South. The monochromatic $H\alpha$ map shows intense emission where the bar is located, and

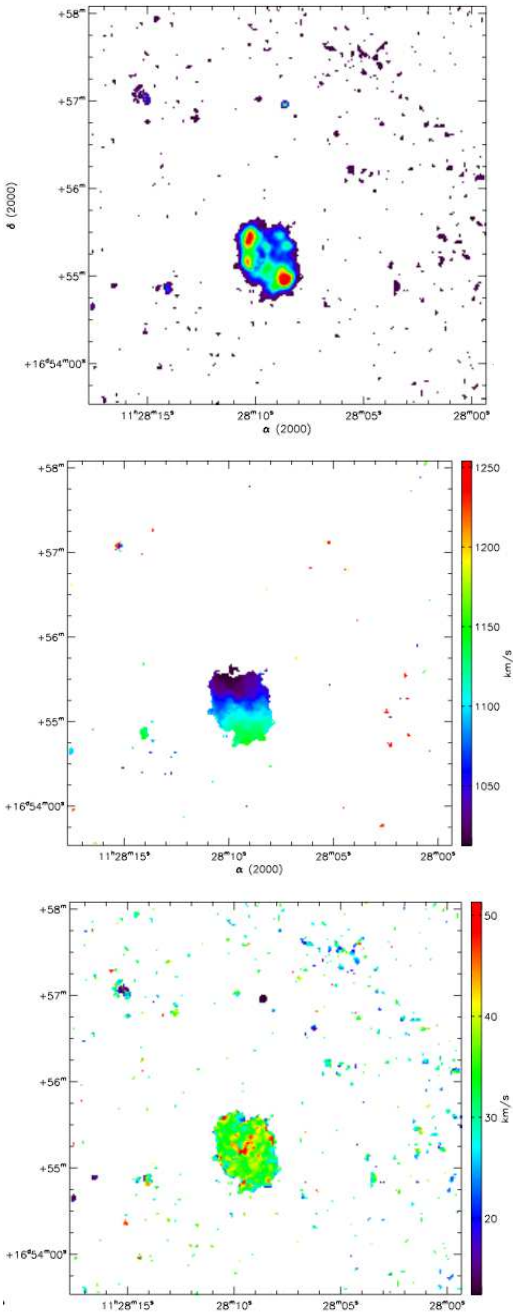


Figure 5. As in Figure 4 for NGC 3691 in U376.

several emission regions as in the *GALEX* image. The velocity dispersion map shows higher dispersion within the bar region. The $H\alpha$ line profiles seem to show a double component on the northern extremity of the galaxy and can be followed to the bar region. $H\alpha$ line profiles do not show multiple components.

UGC 05393 The galaxy presents the most irregular velocity map of the sample. It is classified as an SBd, but the bar is not visible on the velocity field. Emission is mainly present in the emitting regions visible on the UV images. A velocity gradient is present, but the RC (or position velocity) cannot be derived with confidence.

4.2.2 U376: individual kinematical notes

NGC 3655 The velocity field of NGC 3655 is characteristic of a rotating disk with a radial velocity amplitude ranging from 1280 to 1550 km s^{-1} . The map shows a sharp rise in velocity in the centre and a plateau extended up to 25'' from the centre on the blue-shifted side and 38'' on the red-shifted side. Even though the velocity map is very regular, it is not symmetric. $H\alpha$ line profiles, throughout the galaxy, are symmetric without signature of multiple components. The monochromatic $H\alpha$ map shows a non uniform emission for the ionized gas. Two distinct bright regions are visible near the centre, corresponding to a polar ring-like structure. Furthermore, a tail of ionized gas is visible, both from the monochromatic map and from the velocity field, in the East side of the galaxy. The velocity dispersion map shows a high dispersion toward the centre, with values between 60 and 70 km s^{-1} . The RC in figure 6 shows a maximum velocity of 165 km s^{-1} and then a plateau extending almost up to 30'' (3.5 kpc). Although the approaching and receding sides of the RC match well, the curve is not totally symmetric.

NGC 3659 The velocity field of NGC 3659 shows the rotation of a disk, but the plateau is not as extended as in NGC 3655. The velocity map does not show the classical spider pattern. Iso-velocities are not aligned with the major axis of the map. On the blue-shifted side, they are almost straight. $H\alpha$ single component line profiles are very symmetric. The monochromatic $H\alpha$ map shows strong emission regions on the NE of the galaxy. These large regions in that area may be responsible for the behaviour of the velocity field. Interestingly, on the velocity dispersion map, high dispersion is present on the edge of the high emission regions, on the North. The lowest velocity dispersion corresponds to high emission regions. The RC shows almost the same extension of NGC 3655, but the shape is quite different. The RC rises slowly toward a maximum velocity of 85 km/s . A small plateau is present after 20'' (1.6 kpc). The RC is not totally symmetric. A small bump is visible at 22'' (18kpc), the velocity raising to 85 km/s , but no peculiar features can be seen on the velocity map. In the inner 9'' (0.8kpc), the two sides do not agree, probably due to the effect of the bar.

NGC 3684 The velocity field of NGC 3684 is not as typical and regular as NGC 3655. Nevertheless, it shows a clear disk rotation pattern. Iso-velocity contours are almost straight toward the centre (as expected for a typical rotating disk). The position angle of the iso-velocities is not constant along the velocity field major axis. The pattern is particularly visible on the blue-shifted side. $H\alpha$ map shows several bright emission regions, limited to the central part of the galaxy, and few HII regions around the disk. The ionized gas velocity dispersion is low (between 30 to 45 km/s) compared to NGC 3659 for example. It is not obvious, as for NGC 3659, that HII regions are located where the velocity dispersion is lower. $H\alpha$ emission lines do not show multiple components. Despite a peculiar velocity field, both sides of the RC agree remarkably well. The RC raises sharply starting from the inner 10'' (0.7 kpc) to reach a small plateau of about 100 km s^{-1} stable for more than 10'' (1.4 kpc). After that, the curve continues slowly to raise up to 150 km s^{-1} at 50'' (3.6 kpc). The plateau might be due to the presence of two bright HII regions on both side.

NGC 3686 The velocity field of the galaxy is also

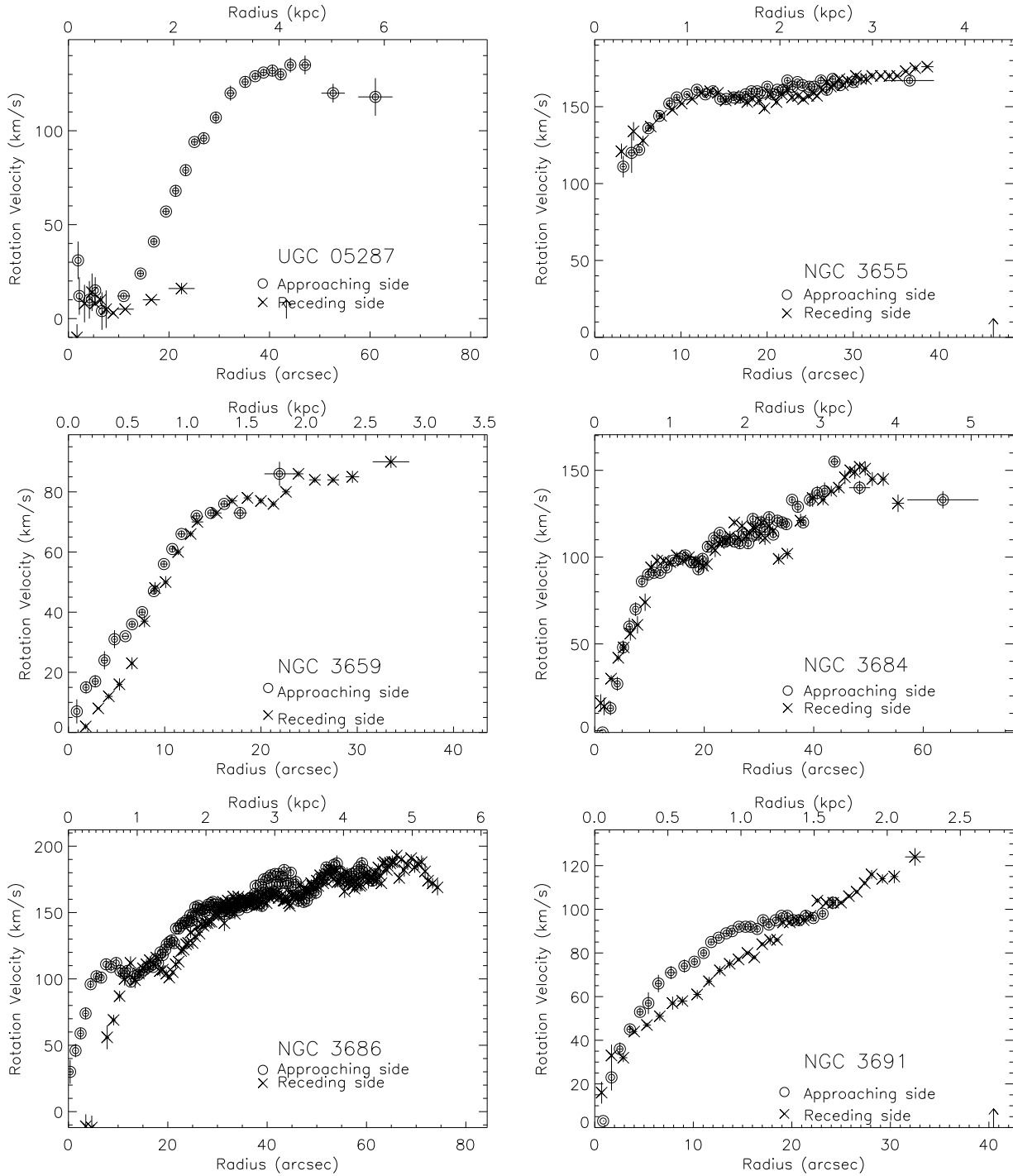


Figure 6. Rotation curves, extracted from 2D velocity fields, of spirals in U268 and U376.

characteristic of a rotating disk. The field is quite symmetric and no distortions are present (such as, large variation of the position angle versus radius), except on the centre where we can notice a distortion due to the presence of the bar. The $H\alpha$ monochromatic image shows bright HII regions along the spiral arms. Those regions are well defined in the UV image (see Figure 3). This galaxy is the only one showing a bright emission in the bulge. The small regions on the South are part of the lower spiral arm visible on the UV image. The bar is barely visible on the $H\alpha$ image. Contrary to the other galaxy, high velocity dispersion corresponds to high intensity

$H\alpha$ emission. Dispersion map shows a velocity dispersion of 75 km s^{-1} in the centre, while has values around $35\text{--}38 \text{ km s}^{-1}$ in the rest of the galaxy. $H\alpha$ line profiles on the central area are broader than elsewhere but they are symmetric, without signature of multiple components. The region of high velocity dispersion is roughly coincident with the location of the bar. The RC shows the two side of the RC differ in the inner $12''$ (1 kpc), then agree almost perfectly to the end of the curve at $70''$ (5 kpc). The influence of the bar certainly plays a role in the disagreement of both side of the RC.

Table 6. Kinematical parameters

Group Galaxies	V_{sysFP} kms^{-1}	PA_{Kin} [deg]	i_{Kin} [deg]
U268			
UGC 5287	1517±5	-	-
UGC 5393	1963±3	153±3	12±15
U376			
NGC 3655	1441±6	27±4	51±1
NGC 3659	1274±2	58±2	62±3
NGC 3684	1117±1	117±1	51±3
NGC 3686	1146±5	17±4	27±2
NGC 3691	1073±1	9 ±1	37±11

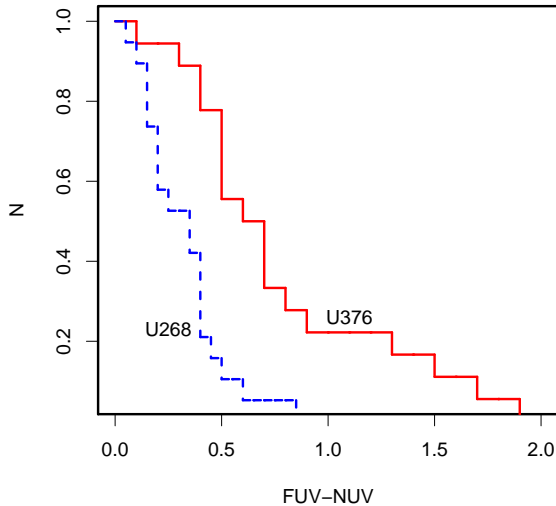


Figure 7. Cumulative distributions of FUV - NUV colours of galaxies in U268, U376. According to a Kolmogorov Smirnov test, the null hypothesis that the two distribution are drawn from the same parent distribution can be rejected at a confidence level > 99%.

NGC 3691 The velocity field confirms the presence of a bar. $H\alpha$ line profiles are symmetric across the galaxy and there are no signatures of multiple components. The $H\alpha$ monochromatic map shows several emission regions possibly on the spiral arms. Contrary to NGC 3686, no emission is detected in the bulge. Velocity dispersion map shows a higher value in the centre (around 50 km s^{-1}), and $\approx 35 \text{ km s}^{-1}$ elsewhere. The region where the dispersion is higher corresponds to the bar. The two sides of the **folded RC differ between $\approx 4''$ (0.5 kpc) and $\approx 20''$ (1.4 kpc).**

5 DISCUSSION

5.1 U268 and U376 as evolving groups

U268 and U376 are dynamically different since their velocity dispersion differs by a factor ~ 4 (65 vs. 230 km s^{-1}). The morphological classification shows that U268 does not contain elliptical galaxies; the overall population of ETGs is composed by S0s only, which are about 24% of the total population. This fraction is comparable with that found for S0s in the general field by Calvi et al. (2012). However, Calvi et al. (2012) found that Ellipticals are at least 20% of the galaxy population even in the less massive environments.

ETGs in U376 represent about 38% of the galaxy population, lower than the average (46%) found for ETGs in field (Calvi et al. 2012). Our groups are then likely representative of very loose galaxy associations. Notice from Figure 1 (bottom left panels), that, at least in projection, U268 has a dispersed configuration at odds with U376 which is more compact than many other groups in the region and which, not surprisingly, show a larger fraction of ETGs.

Figure 7 shows the cumulative distributions of FUV-NUV colours of galaxies in U268 and U376. The distribution gives the fraction of galaxies in each group having a colour greater (redder) than a given value of FUV-NUV. E.g. $\sim 10\%$ of galaxies in U268 has $FUV-NUV > 0.5$ AB mag while in U376 they are nearly 80%. Using a Kolmogorov-Smirnov two-sample test, we tested the null hypothesis that the two distributions come from the same population, finding that they are different (confidence level > 99%), galaxies in U268 being bluer than those in U376.

In Figure 8 we show the UV - optical CMDs of members of the two groups.

In U268, the ‘red sequence’, where passively evolving galaxies are located, is completely unpopulated. Even S0s (yellow squares), like MRK 408, populate either the ‘blue sequence’ or the ‘green valley’. Most of the galaxies lie in the ‘blue sequence’. Many bright spiral galaxies show signature of interaction or morphological distortions (encircled symbols in Figure 8). The spiral NGC 3067, lying in the ‘green valley’, is the reddest of the bright members.

On the contrary, U376 shows a well defined ‘red sequence’ populated by both ellipticals and S0s. Also the shell galaxy NGC 3605 is located in the ‘red sequence’. Since an accretion event is believed to produce shells (Dupraz & Combes 1987), the latter have been likely produced by a dry accretion that did not ignite star formation or the galaxy already come back to the ‘red sequence’ if shells are long lasting (e.g. Longhetti et al. 2000). Line strength indices of NGC 3607 (Rampazzo et al. 2005; Annibali et al. 2006) have been used to compute the luminosity weighted age, metallicity and $[\alpha/Fe]$ enhancement of the galaxy. Annibali et al. (2007) report a luminosity weighted age of 3.1 ± 0.5 Gyr for NGC 3607, high metallicity (Z_{\odot} , nearly two times solar 0.047 ± 0.012) and $[\alpha/Fe] = 0.24 \pm 0.03$. The age suggests that the galaxy may have had a recent star formation episode. The galaxy shows emission lines with LINER characteristics (Annibali et al. 2010). Notwithstanding, NGC 3607 lies in the ‘red sequence’ (see also Marino et al. 2011, for the photometry of the inner regions $r_e/8$). This fact is not unexpected: far-UV colours are very sensitive to recent ($< 1\text{Gyr}$) star formation episodes

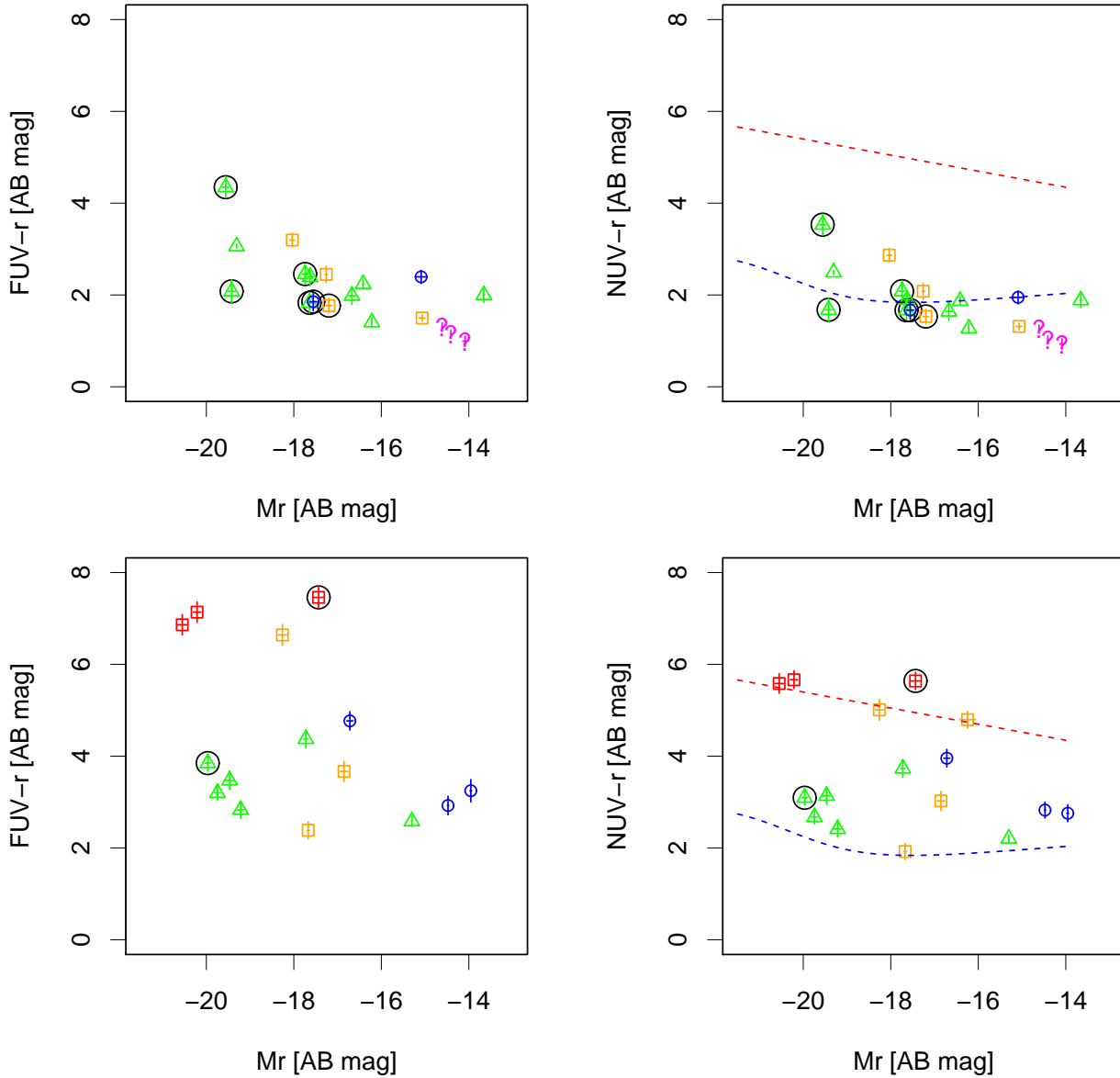


Figure 8. (Top) UV - optical CMDs of the members in U268. (M_r vs. FUV -r (left), M_r vs. NUV -r (right)). (Bottom): as top panels for U376 members. In the M_r vs. NUV-r CMD, we overplot the Wyder et al. (2007) fits to the red and blue galaxy sequences. Triangles indicate spirals, squares early-type galaxies (red Ellipticals and yellow S0s), circles irregulars. ‘?’ indicate galaxies without morphological classification (see our revised classification in Table 3). Encircled symbols indicate galaxies with interaction signatures. Magnitudes of all galaxies but SDSSJ095430.02+320342.0 were corrected by galactic extinction.

(e.g. Rampazzo et al. 2007; Bianchi 2011), line-strength indices may trace better older episodes. Late-type galaxies are not found in the ‘blue sequence’ but in the ‘green valley’. Only NGC 3655 shows signature of on-going interaction but it shares with the other spirals the ‘green valley’ region.

Figure 9 shows the galaxies of the group LGG 225 (Garcia 1993), also belonging to the Leo cloud (Figure 1 right bottom panel) in the (M_r vs. NUV-r) plane, using the NUV and SDSS-r photometry published in Paper I. Some

LGG 225 members display interacting and distorted morphologies particularly evident in the UV images. UV colors suggest very recent episodes of star formation triggered by recent and on-going interaction. In the (M_r vs. NUV-r) plane, the phase of LGG 225 appears intermediate between U268 and U376. The two Ellipticals, located in the ‘red sequence’, are not the most massive and luminous galaxies in the group. No S0s are present. The ‘blue sequence’ is pop-

ulated by star forming and interacting galaxies. There is a large fraction ($\simeq 40\%$) of galaxies in the ‘green valley’.

Summarising we suggest that in different regions of the Leo cloud the majority of galaxies, irrespective of their morphological type, are experiencing a transformation. In particular, in U376 this transformation brings the galaxies to the ‘green valley’.

5.2 Transforming mechanisms

In U268 the galaxies that show signature of interaction are all Spirals (NGC 3003, UGC 5287, UGC 5326, NGC 3067, PGC028169 and UGC 5093). All these galaxies but NGC 3067, that inhabits the ‘green valley’, are located in the ‘blue sequence’.

The kinematics of NGC 3003 and NGC 3067 have been studied by Epinat et al. (2008b). They found that the $H\alpha$ emission in NGC 3003 is rather faint and have an asymmetric distribution as if the galaxy was disturbed by a dwarf companion. Also the velocity field is rather asymmetric. Epinat et al. (2008b) found the signature of a bar in the velocity field of NGC 3607. This galaxy is seen nearly edge-on with dust patchy structure in its centre (Carollo et al. 1998). Interaction signatures are visible in the 2MASS images (Jarrett et al. 2000): a tidal arm/tail is detected in the SE direction. This arm/tail appears closed as a ring in the SDSS image of Figure 2, while the nucleus is displaced to the NW with respect to the centre of the ring.

The 2D kinematics of two additional spiral members (UGC 5287 and UGC 5393) analysed here, shows that both galaxies are barred, although the bar signatures are not visible in the velocity field of UGC 5393. In UGC 5287 we detect a double component $H\alpha$ profile from the northern galaxy outskirts to the bar region, likely a signature of an infalling gas component. Rampazzo et al. (2006) interpreted a similar feature in the interacting spiral NGC 470 as signature of infalling gas. If we consider the southern bright region as a possible companion, the rotation curve can be separated in two parts, the northern one, typical of a disk galaxy, and the southern one, very irregular indicating that the companion has a disturbed motion.

We find that NGC 3011 and UGC 5326 both have a ring structure. Gil de Paz et al. (2003) found that NGC 3011 has an inner and an outer ring. They suggest that the inner disk could be produced by a starburst-driven shock interacting with the surrounding interstellar medium. Comerón et al. (2010) classify the galaxy as a S0a, and did not find a signature of bar, which is generally connected to the presence of rings. UGC 5326 may be suffer a head-on collision.

Also S0s lie in the ‘blue sequence’: they are blue compact dwarfs, like MRK 408 (Hunter & Elmegreen 2004) with an intense nuclear star formation and even “Wolf-Rayet (WR) galaxies” as IC 2524 (MRK 411), i.e. galaxies with signature of very recent star formation (WR stars appear 2×10^6 years after a star formation episode and disappear within some 5×10^6 (Brinchmann et al. 2008). Dwarf early-type galaxies may have acquired gas by interaction with a gas rich donor as mentioned above in the case of the velocity field of NGC 3003 (see e.g. Rampazzo et al. 1995; Domingue et al. 2003).

Summarising, the main evolutionary mechanism at work in U268 is the interaction/collision between galaxies

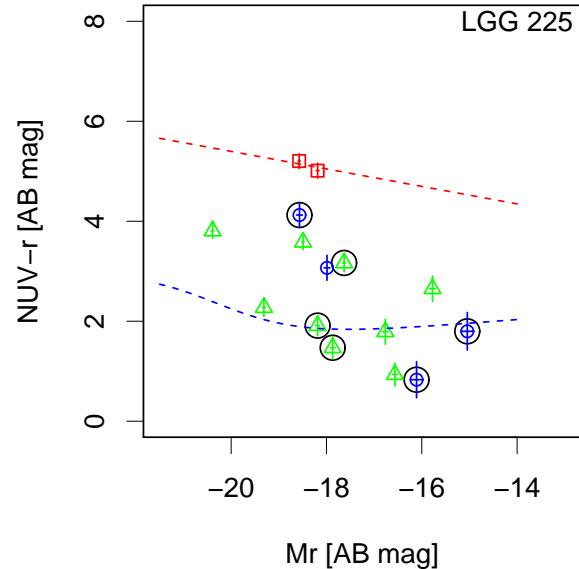


Figure 9. M_r vs. $NUV-r$ for the LGG 225 association (see Marino et al. 2010) which is also part of the Leo cloud as shown in Figure 1 mid right panel. Symbols are as in Figure 8.

which could lead to the generation of bars and rings, possibly igniting a star formation episode (Noguchi 1990). Kinematical studies confirm such picture showing that both asymmetries in the velocity field and bar are common features in the Spirals of the group.

U376, which appears more concentrated than U268, shows a larger number of ETGs. We refer to a forthcoming paper for the analysis of the SEDs of ETGs, that will give us further insight into the processes driving their evolution.

NGC 3626 presents an extended gas counterrotation (Ciri et al. 1995), with ionized and atomic hydrogen rotating in opposite direction to the stars. Emsellem et al. (2004) shows that the velocity field of NGC 3608 displays the presence of a counter-rotating core (Jedrzejewski & Schechter 1988; Halliday et al. 2001) in the central region (inner $8''$). Counterrotations are widely interpreted as generated by accretion events (Galletta 1996; Corsini & Bertola 1998). Neither in NGC 3605 nor in NGC 3608 CO has been detected (Sage et al. 2007). Mid infrared Spitzer-IRS spectra of NGC 3608 show that the galaxy is passively evolving, without PAH emission (Rampazzo et al. 2012, in prep.). NGC 3608 has a low X-ray luminosity 2.7×10^{39} erg s^{-1} (David et al. 2006) and does not show an AGN activity although there has been a past “activity” witnessed by the presence of cavities in the X-ray emission (Cavagnolo et al. 2010).

A tentative picture of the ETGs evolution in U376 may be connected to accretion episodes that leave their morphological, kinematical, and photometric (young age of the stellar population) imprinted on the ETGs. Moreover, signatures of secular evolution are detected in a large fraction

of Spirals. There is a larger presence of bars with respect to U268 (29% vs. 10%). The bar signature is detected also in the velocity field together with several kinds of asymmetries as described in Section 4.2. Only NGC 3655 shows recent/on-going interactions. What bring them to the ‘green valley’? Can be the higher concentration of the group the answer? The study of Sengupta & Balasubramanyam (2006) about the HI content of galaxies in loose groups give us further insight about this point. These authors compute the HI deficiency of each galaxy in the group, as $\text{def}_{HI} = \log \frac{(M_{HI})_{pred}}{D^2} - \log \frac{(M_{HI})_{obs}}{D^2}$, with M_{HI} in solar masses and D , the RC3 galaxy diameter, in kpc. The average of the predicted (Sengupta & Balasubramanyam 2006) minus the observed HI surface densities of all the galaxies of a group is used as a measure of the HI deficiency of the group.

They found that galaxies in groups with diffuse X-ray emission, on average, are HI deficient, and have lost more gas compared to those in groups without X-ray emission. The group U376 is included in the Sengupta & Balasubramanyam (2006) study (NGC 3686 in their Table 3) among groups with diffuse X-ray emission. Their 21 members correspond, with three exceptions, to our independent list reported in Table 1. A large fraction of spirals/Irr in the list (UGC 6296, UGC 6341, NGC 3592, PGC 035087, PGC 35096, NGC 3686 and NGC 3691) are HI deficient. Conversely, UGC 6320, NGC 3659, NGC 3655, NGC 3681, NGC 3684 show an excess of HI. Sengupta & Balasubramanyam (2006) suggest that tidal aided ram-pressure stripping and evaporation are the possible mechanisms leading to the excess gas loss found in groups with diffuse X-ray. U376 as a whole is only barely HI deficient (0.07 ± 0.062) but single galaxies are likely undergoing a transformation by mechanisms sketched above.

We estimated the HI deficiency of U268, using the HI flux of the galaxy members given in NED (Springob et al. 2005; Huchtmeier & Richter 1989; Schneider et al. 1990). We find that the spirals UGC 5446 and NGC 3118, ~ 1.6 Mpc apart from the center of the group are the HI richest members, while NGC 3067 and UGC 05282 are HI deficient. NGC 3003, UGC 05287, UGC 5326 have def_{HI} of about -0.05, 0.05 and 0.01 respectively. The def_{HI} of the group U268 is ~ -0.01 .

6 SUMMARY

We have presented the photometric and kinematic analysis of U268 and U376, two galaxy groups in the Leo cloud. Starting from the membership of the two groups defined in Ramella et al. (2002), we enriched the original group with members sharing the same spatial and velocity extent given in the HYPERLEDA database. The velocity dispersion of the two groups differs by a factor ~ 4 (67 vs. 240 kms^{-1} in U268 and U376 respectively). U268 does not contain Ellipticals, the overall population of ETGs is composed by S0s only, which are a small (24%) fraction of the total, and comparable with that found in the field (Calvi et al. 2012). ETGs in U376 are 38% of the total whose 8% of Ellipticals and 30% of S0s. We investigated the presence of substructures and the environment of each group. We find substructure to be evident from the Dressler-Shectman test in both groups. Galaxy members of U376 have a more compact configuration

than U268 with the surrounding of U376 richer of galaxies and crowded by tight associations.

We obtained the FUV and NUV (*GALEX*) and optical (SDSS) surface photometry of bright members and integrated photometry of all members. We have also obtained 2D kinematics of a set of bright spirals in the two groups looking for distortions in the velocity field resulting from galaxy-galaxy interaction. A large fraction of galaxies in U268 shows interaction signatures (60% vs. 13%) both from their photometry and kinematics.

(FUV - NUV) colours of galaxies in U268 are bluer than those in U376. No galaxies are populating the ‘red sequence’ of U268, all lying in the ‘blue sequence’ and in the ‘green valley’, including S0s. At odds, the ‘blue sequence’ of U376 is un-populated with respect to U268, and a large set of galaxies populates the ‘green valley’. At the same time, very few galaxies in U376 show a distorted morphology due to on-going interactions. Sengupta & Balasubramanyam (2006) show that U376 members are, at least partly, depleted of gas. We estimate that the members of U268 are less deficient in HI than U376. Galaxy-galaxy interaction and gas removal seem the basic mechanisms leading the transformation of late-type galaxies in our groups in Leo. ETGs in U376 show signatures of past accretion events, e.g. shells, stellar population rejuvenation, counter rotating core. **The presence of rings, likely connected to the internal secular evolution (e.g. NGC 3011 in U268, NGC 3681 in U376), polar rings produced by minor/major accretion events and collisional rings recognizable from the off-centered nucleus (e.g. UGC 5326 in U268, UGC 6320 in U376), have been found.**

We also compared the CMDs of the two groups analysed here with LGG225, a group for which comparable measurements are available in Paper I. U268 is likely in a early evolutionary stage in comparison to U376, with LGG225 in between.

In a forthcoming paper we will use the multi-wavelength SEDs and the kinematics data presented here to obtain (1) the star formation history and the stellar masses of ETGs using chemo-photometric SPH models (see Bettoni et al. 2011), (2) the stellar and kinematic masses of spiral members, (3) a luminosity-weighted kinematical and dynamical analysis of each group. We will also expand the study to other 11 groups, with a wide range of characteristics (in richness of members, velocity dispersions, morphological types) for which we have UV and optical images.

ACKNOWLEDGMENTS

A.M. and L.B. acknowledge support from NASA grant NNX10AM36G. A.M., R.R., D.B., L.B., and P.M. acknowledge financial contribution from the agreement ASI-INAF I/009/10/0. This work has been partially supported by the Padova University funds 2011/12 (ex 60%). M. R. acknowledges support from grants P-82389 from CONACYT and IN102309 from DGAPA-UNAM. *GALEX* is a NASA Small Explorer, launched in April 2003. This work is based on *GALEX* GI data from program G16 - 6017 and *GALEX* archival data taken from MAST (<http://galex.stsci.edu>). STScI is operated by the Association of Universities for Research in Astronomy, Inc., under NASA contract NAS5-

26555. Support for MAST for non-HST data is provided by the NASA Office of Space Science via grant NAG5-7584 and by other grants and contracts. We acknowledge the usage of the HYPERLEDA (<http://leda.univ-lyon1.fr>) and NED databases. **We thank the anonymous referee for useful comments which helped to improve the paper.**

Facilities: GALEX, Sloan

REFERENCES

- Adelman-McCarthy J. K., Agüeros M. A., Allam S. S., Al-
lende Prieto C., Anderson K. S. J., Anderson S. F., Annis
J., Bahcall N. A., 2008, *ApJS*, 175, 297
- Amram P., Balkowski C., Boulesteix J., Cayatte V.,
Marcelin M., Sullivan, III W. T., 1996, *A&A*, 310, 737
- Annibali F., Bressan A., Rampazzo R., Zeilinger W. W.,
2006, *A&A*, 445, 79
- Annibali F., Bressan A., Rampazzo R., Zeilinger W. W.,
Danese L., 2007, *A&A*, 463, 455
- Annibali F., Bressan A., Rampazzo R., Zeilinger W. W.,
Vega O., Panuzzo P., 2010, *A&A*, 519, A40
- Bai L., Rasmussen J., Mulchaey J. S., Dariush A., Ray-
chaudhury S., Ponman T. J., 2010, *ApJ*, 713, 637
- Baldry I. K., Glazebrook K., Brinkmann J., Ivezić Ž., Lup-
ton R. H., Nichol R. C., Szalay A. S., 2004, *ApJ*, 600,
681
- Balogh M. L., Baldry I. K., Nichol R., Miller C., Bower R.,
Glazebrook K., 2004, *ApJ*, 615, L101
- Barnes E. I., Sellwood J. A., 2003, *AJ*, 125, 1164
- Barnes J. E., 1996, *Dynamics of Galaxy Interactions*, Ken-
nicutt Jr. R. C., Schweizer F., Barnes J. E., eds., p. 275
- Barnes J. E., 2002, *MNRAS*, 333, 481
- Bettoni D., Galletta G., Rampazzo R., Marino A., Mazzei
P., Buson L. M., 2011, *A&A*, 534, A24
- Bianchi L., 2009, *Ap&SS*, 320, 11
- Bianchi L., 2011, *Ap&SS*, 335, 51
- Brinchmann J., Kunth D., Durret F., 2008, *A&A*, 485, 657
- Calvi R., Poggianti B. M., Fasano G., Vulcani B., 2012,
MNRAS, 419, L14
- Cardelli J. A., Clayton G. C., Mathis J. S., 1989, *ApJ*, 345,
245
- Carollo C. M., Stiavelli M., Mack J., 1998, *AJ*, 116, 68
- Cavagnolo K. W., McNamara B. R., Nulsen P. E. J., Carilli
C. L., Jones C., Birzan L., 2010, *ApJ*, 720, 1066
- Ciri R., Bettoni D., Galletta G., 1995, *Nature*, 375, 661
- Comerón S., Knapen J. H., Beckman J. E., Laurikainen E.,
Salo H., Martínez-Valpuesta I., Buta R. J., 2010, *MNRAS*,
402, 2462
- Corsini E. M., Bertola F., 1998, *Journal of Korean Physical
Society*, 33, 574
- Daigle O., Carignan C., Hernandez O., Chemin L., Amram
P., 2006, *MNRAS*, 368, 1016
- David L. P., Jones C., Forman W., Vargas I. M., Nulsen
P., 2006, *ApJ*, 653, 207
- Di Matteo T., Springel V., Hernquist L., 2005, in *Growing
Black Holes: Accretion in a Cosmological Context*,
A. Merloni, S. Nayakshin, & R. A. Sunyaev, ed., pp. 340–
345
- Domingue D. L., Sulentic J. W., Xu C., Mazzarella J., Gao
Y., Rampazzo R., 2003, *AJ*, 125, 555
- Dressler A., Shectman S. A., 1988, *AJ*, 95, 985
- Dupraz C., Combes F., 1986, *A&A*, 166, 53
- Dupraz C., Combes F., 1987, *A&A*, 185, L1
- Eke V. R., Baugh C. M., Cole S., Frenk C. S., Norberg P.,
Peacock J. A., 2004, *MNRAS*, 348, 866
- Ellison S. L., Patton D. R., Simard L., McConnachie A. W.,
2008, *AJ*, 135, 1877
- Ellison S. L., Patton D. R., Simard L., McConnachie A. W.,
Baldry I. K., Mendel J. T., 2010, *MNRAS*, 407, 1514
- Emsellem E. et al., 2004, *MNRAS*, 352, 721
- Epinat B., Amram P., Marcelin M., 2008a, *MNRAS*, 390,
466
- Epinat B., Amram P., Marcelin M., Balkowski C., Daigle,
O e. a., 2008b, *MNRAS*, 388, 500
- Firth P., Evstigneeva E. A., Jones J. B., Drinkwater M. J.,
Phillipps S., Gregg M. D., 2006, *MNRAS*, 372, 1856
- Galletta G., 1996, in *Astronomical Society of the Pa-
cific Conference Series*, Vol. 91, IAU Colloq. 157: Barred
Galaxies, Buta R., Crocker D. A., Elmegreen B. G., eds.,
p. 429
- Garcia A. M., 1993, *A&AS*, 100, 47
- Geller M. J., Huchra J. P., 1983, *ApJS*, 52, 61
- Gil de Paz A., Madore B. F., Noeske K., Cairós L. M.,
Papaderos P., Silich S. A., 2003, *ApJ*, 596, L179
- Halliday C., Davies R. L., Kuntschner H., Birkinshaw M.,
Bender R., Saglia R. P., Bagglely G., 2001, *MNRAS*, 326,
473
- Hou A., Parker L. C., Harris W. E., Wilman D. J., 2009,
ApJ, 702, 1199
- Hou A. et al., 2012, *MNRAS*, 421, 3594
- Huchtmeier W. K., Richter O.-G., 1989, *A General Catalog
of HI Observations of Galaxies. The Reference Catalog.*
- Hunter D. A., Elmegreen B. G., 2004, *AJ*, 128, 2170
- Jarrett T. H., Chester T., Cutri R., Schneider S., Skrutskie
M., Huchra J. P., 2000, *AJ*, 119, 2498
- Jedrzejewski R., Schechter P. L., 1988, *ApJ*, 330, L87
- Jedrzejewski R. L., 1987, *MNRAS*, 226, 747
- Kawata D., Mulchaey J. S., 2008, *ApJ*, 672, L103
- Kenicutt, Jr. R. C., Schweizer F., Barnes J. E., 1996,
Galaxies: Interactions and Induced Star Formation
- Lacey C., Cole S., 1993, *MNRAS*, 262, 627
- Laval A., Boulesteix J., Georgelin Y. P., Georgelin Y. M.,
Marcelin M., 1987, *A&A*, 175, 199
- Lewis I., Balogh M., De Propriis R., Couch W., et al., 2002,
MNRAS, 334, 673
- Longhetti M., Bressan A., Chiosi C., Rampazzo R., 2000,
A&A, 353, 917
- Mamon G. A., 1992, *ApJ*, 401, L3
- Marino A., Bianchi L., Rampazzo R., Buson L. M., Bettoni
D., 2010, *A&A*, 511, A29
- Marino A., Bianchi L., Rampazzo R., Thilker D. A., Anni-
bali F., Bressan A., Buson L. M., 2011, *ApJ*, 736, 154
- Martin D. C., Fanson J., Schiminovich D., et al., 2005, *ApJ*,
619, L1
- Martin D. C. et al., 2007, *ApJS*, 173, 342
- McCarthy I. G., Frenk C. S., Font A. S., Lacey C. G.,
Bower R. G., Mitchell N. L., Balogh M. L., Theuns T.,
2008, *MNRAS*, 383, 593
- Moiseev A. V., Bizyaev D. V., 2009, *New A Rev.*, 53, 169
- Morrissey P., Conrow T., Barlow T. A., Small T., Seibert
M., Wyder T. K., Budavári, 2007, *ApJS*, 173, 682
- Noguchi M., 1990, *Bar formation in interacting galaxies
and the fueling of nuclei.*, Wielen, R., ed., pp. 469–472

Paturel G. et al., 1997, *A&AS*, 124, 109
 Paturel G., Petit C., Prugniel P., Theureau G., Rousseau J., Brouty M., Dubois P., Cambr esy L., 2003, *A&A*, 412, 45
 Petrosian A., McLean B., Allen R. J., MacKenty J. W., 2007, *ApJS*, 170, 33
 Ramella M., Geller M. J., Pisani A., da Costa L. N., 2002, *AJ*, 123, 2976
 Rampazzo R. et al., 2006, *MNRAS*, 368, 851
 Rampazzo R., Annibali F., Bressan A., Longhetti M., Padoan F., Zeilinger W. W., 2005, *A&A*, 433, 497
 Rampazzo R. et al., 2007, *MNRAS*, 381, 245
 Rampazzo R., Reduzzi L., Sulentic J. W., Madejsky R., 1995, *A&AS*, 110, 131
 Rasmussen J., Ponman T. J., Mulchaey J. S., 2006, *MNRAS*, 370, 453
 Rosado M. et al., 1995, in *Revista Mexicana de Astronomia y Astrofisica Conference Series*, Vol. 3, *Revista Mexicana de Astronomia y Astrofisica Conference Series*, M. Pena & S. Kurtz, ed., p. 263
 Sage L. J., Welch G. A., Young L. M., 2007, *ApJ*, 657, 232
 Schneider S. E., Thuan T. X., Magri C., Wadiak J. E., 1990, *ApJS*, 72, 245
 Schweizer F., 1996, *Observational Evidence for Interactions and Mergers*, Kennicutt Jr. R. C., Schweizer F., Barnes J. E., eds., pp. 105–274
 Scudder J. M., Ellison S. L., Mendel J. T., 2012, *MNRAS*, 423, 2690
 Sengupta C., Balasubramanyam R., 2006, *MNRAS*, 369, 360
 Silverman B. W., 1986, *Density estimation for statistics and data analysis*
 Springob C. M., Haynes M. P., Giovanelli R., Kent B. R., 2005, *ApJS*, 160, 149
 Strateva I. et al., 2001, *AJ*, 122, 1861
 Tago E., Einasto J., Saar E., Tempel E., Einasto M., Vennik J., M uller V., 2008, *A&A*, 479, 927
 Thomson R. C., 1991, *MNRAS*, 253, 256
 Toomre A., Toomre J., 1972, *ApJ*, 178, 623
 Tully R. B., 1988, *Nearby galaxies catalog*. Cambridge and New York, Cambridge University Press, 1988, 221 p.
 Wyder T. K., Martin D. C., Schiminovich D., Seibert M., Budav ari T., Treyer, M. A. e. a., 2007, *ApJS*, 173, 293
 York D. G. et al., 2000, *AJ*, 120, 1579
 Zabludoff A. I., Mulchaey J. S., 1998a, *ApJ*, 498, L5
 Zabludoff A. I., Mulchaey J. S., 1998b, *ApJ*, 498, L5

est galaxies of U268 and U376 respectively and having a heliocentric radial velocity within $\pm 3\sigma$ of the group mean velocity in the catalog of Ramella et al. (2002).

APPENDIX A: UV AND OPTICAL IMAGES OF THE ADDED MEMBERS OF U268 AND U376

Figures A1 and A2 show the UV and optical colour composite images of the added members of U268 and U376 respectively. The image of PGC2016633 in U268 is shown in Figure 2.

APPENDIX B: ENVIRONMENT OF U268 AND U376

Tables B1 and B2 compile the main characteristics of the galaxies in a box of 4 Mpc \times 4 Mpc centred on the B bright-

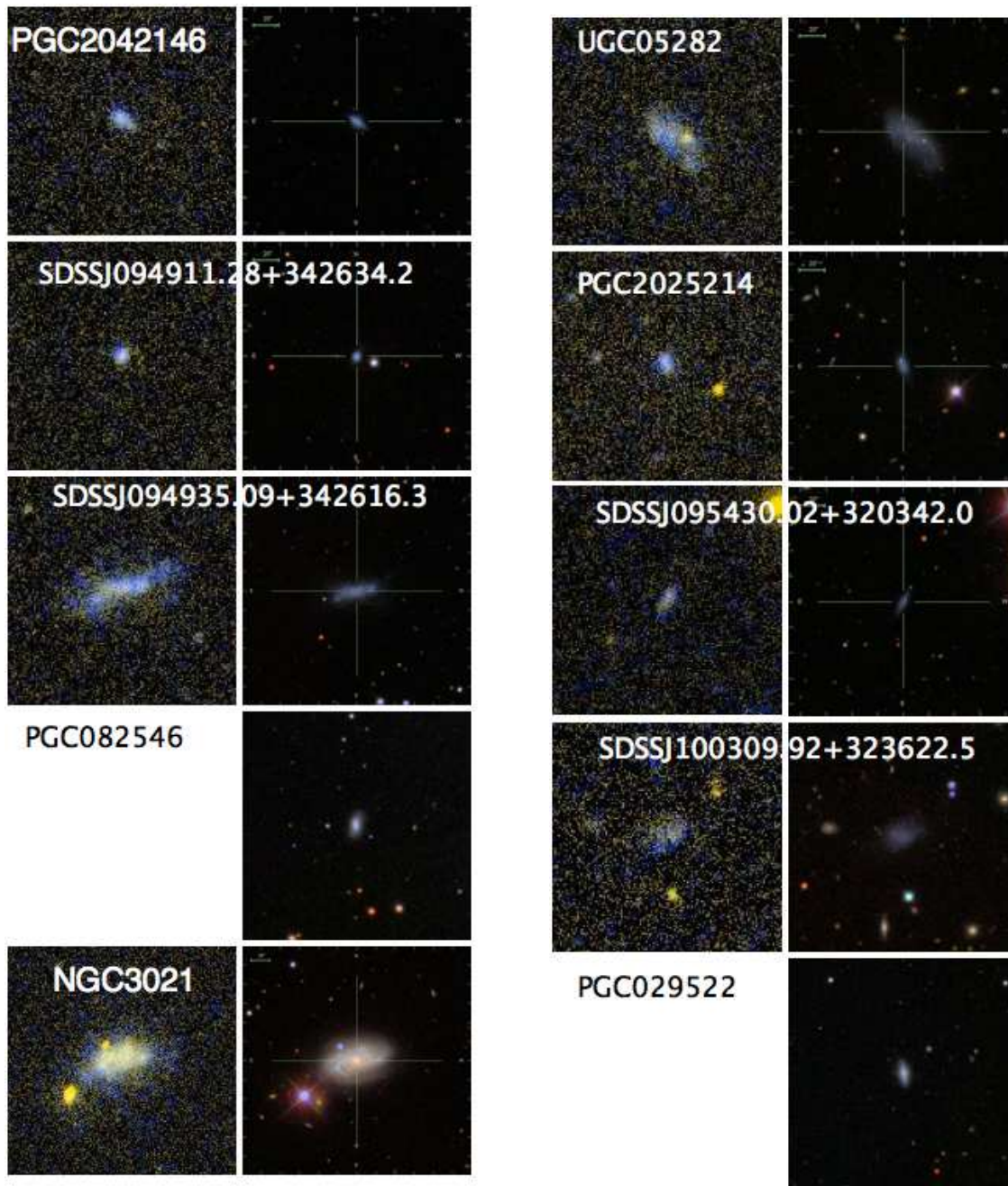


Figure A1. Color composite UV (FUV blue, NUV yellow, first and third panel from left) and optical (SDSS, g blue, r green, i red, second and fourth panel) images of the new member galaxies in U268.

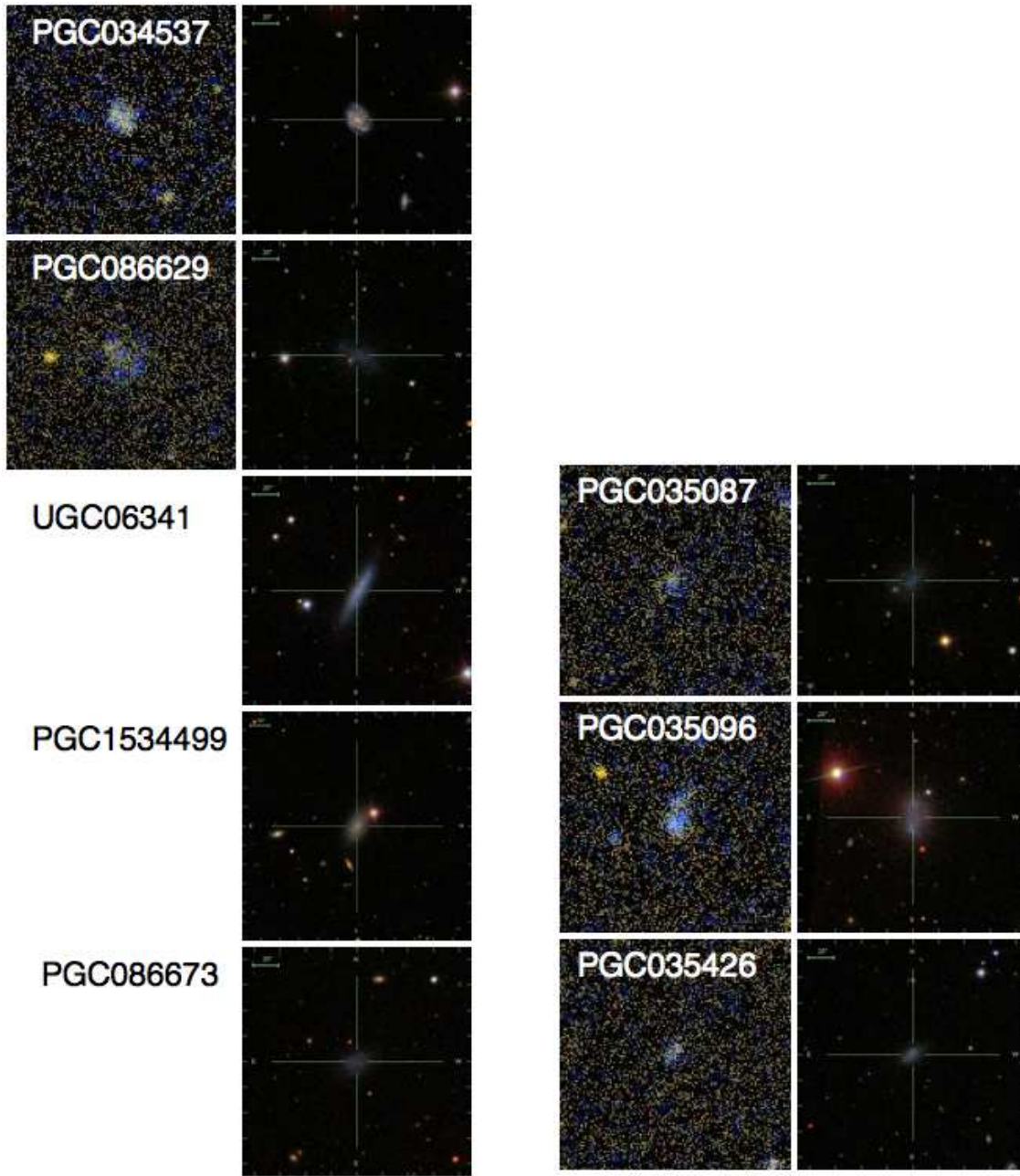


Figure A2. Color composite UV (FUV blue, NUV yellow, first and third panel from left) and optical (SDSS, g blue, r green, i red, second and fourth panel) images of the new member galaxies of U376.

Table B1. Galaxies in a box of 4 Mpc \times 4 Mpc centred on NGC 3003 in U268 with heliocentric radial velocity within $\pm 3\sigma$ of the group mean velocity given in the catalog of Ramella et al. (2002).

Galaxies	RA (J2000) (hours)	Dec. (J2000) (degrees)	Morph. type	Mean Hel. Vel. [km/s]	logD ₂₅ [arcmin]	logr ₂₅	P.A. [deg]	B _T mag
U268								
UGC05015	9.42999	34.2771	7.8	1648 \pm 5	1.21	0.02		15.60 \pm 0.32
UGC05020	9.43374	34.65339	5.8	1619 \pm 7	1.31	0.59	77.6	15.16 \pm 0.27
PGC027157	9.56196	33.60034	-1	1601 \pm 23	0.88	0.14	127.2	15.57 \pm 0.31
SDSSJ093441.75+323203.5	9.57826	32.53437		1277 \pm 54			119.6	
UGC05105	9.58888	35.91365	9.9	1588 \pm 7	0.99	0.15	147.2	16.11 \pm 0.50
PGC027311	9.60209	29.11222	3.5	1652 \pm 2	0.87	0.42	8.5	15.62 \pm 0.45
SDSSJ094029.36+365443.5	9.67482	36.91214	10	1629 \pm 63	0.58	0.07	7.1	17.76 \pm 0.50
PGC027626	9.6794	32.47254		1288 \pm 3	0.31	0.06	82.4	18.03 \pm 0.50
NGC2964	9.71512	31.84703	4.1	1318 \pm 3	1.47	0.13	97	12.04 \pm 0.09
SDSSJ094254.50+315103.5	9.71515	31.85104		1321 \pm 36				
NGC2968	9.72	31.92873	1.2	1556 \pm 13	1.39	0.18	54	12.74 \pm 0.09
SDSSJ094316.02+313725.1	9.72111	31.62357		1541 \pm 91			73.4	
PGC2832070	9.72196	31.82409		1468 \pm 68			90.4	
NGC2970	9.7253	31.9769	-4.6	1644 \pm 15	0.93	0.06	64.8	14.41 \pm 0.11
PGC1973445	9.72571	31.96755		1416 \pm 90	0.63	0.23	71.4	17.89 \pm 0.50
SDSSJ094338.13+351207.8	9.72726	35.2022		1552 \pm 41	0.53	0.2	93.8	17.77 \pm 0.50
PGC027992	9.7637	30.53404	4.8	1495 \pm 34	0.48	0.26	39	18.10 \pm 0.50
PGC028086	9.78139	31.79583		1396 \pm 42	0.4	0.1		18.39 \pm 0.50
PGC028153	9.79657	39.08419	3.9	1592 \pm 9	0.68	0.04	129.8	15.20 \pm 0.15
PGC2800953	9.79722	39.1427		1553 \pm 25				
SDSSJ094758.45+390510.1	9.79957	39.0862	10	1501 \pm 60	0.6	0.28	112.1	18.09 \pm 0.35
PGC2016633	9.80076	32.90034		1552 \pm 47	0.63	0.21	165	17.25 \pm 0.50
PGC028169	9.8013	32.88255	3.2	1528 \pm 7	0.83	0.11	163.9	14.76 \pm 0.28
PGC1916762	9.80591	30.75928		1468 \pm 5	0.43	0.08	26.6	18.48 \pm 0.50
SDSSJ094829.55+332459.3	9.8082	33.41643		1619 \pm 338			82	
NGC3003	9.80992	33.42136	4.3	1480 \pm 3	1.68	0.65	78.8	12.25 \pm 0.10
SDSSJ094838.45+332529.1	9.8107	33.42466		1419 \pm 31			86.8	
SDSSJ094847.46+275225.4	9.81319	27.8737		1311 \pm 2			38.7	
PGC2042146	9.81754	33.99134		1494 \pm 2	0.5	0.14	53.8	17.85 \pm 0.5
SDSSJ094911.28+342634.2	9.81979	34.44292		1489 \pm 2			164.1	
SDSSJ094935.09+342616.3	9.82641	34.43793		1488 \pm 2			98.3	
NGC3011	9.82811	32.22109	-1.7	1539 \pm 5	0.92	0.08	59.5	14.54 \pm 0.44
PGC028305	9.83635	28.01298	-4.8	1448 \pm 6	0.73	0.09	63.5	15.81 \pm 0.40
SDSSJ095011.18+280044.8	9.83645	28.0125		1458 \pm 32	0.81	0.22	49.8	16.05 \pm 0.35
s PGC082546	9.83917	33.58391	4.6	1586 \pm 29	0.56	0.15	171	17.05 \pm 0.36
NGC3026	9.84871	28.55119	9.7	1488 \pm 4	1.35	0.57	82.7	13.85 \pm 0.43
NGC3021	9.84921	33.55341	4	1540 \pm 3	1.13	0.23	108.3	12.54 \pm 0.27
SDSSJ095058.02+333319.3	9.84946	33.55535		1596 \pm 3			125.7	
UGC05282	9.85284	33.13083	8.8	1557 \pm 10	0.97	0.27	46	
UGC05287	9.8578	32.94288	5.9	1470 \pm 6	0.98	0.12		14.84 \pm 0.42
SDSSJ095141.68+384207.1	9.86158	38.70185	10	1426 \pm 3	0.63	0.02		17.41 \pm 0.35
NGC3032	9.86895	29.23653	-1.9	1538 \pm 6	1.15	0.04		13.07 \pm 0.20
PGC028474	9.88261	29.31088	7.9	1638 \pm 6	0.53	0.26	9.3	17.79 \pm 0.86
PGC2025214	9.8959	33.16437		1520 \pm 35	0.55	0.25	18.5	18.08 \pm 0.50
SDSSJ095430.02+320342.0	9.90835	32.06166		1421 \pm 2			152.9	
UGC05326	9.92349	33.26252	9.8	1413 \pm 3	0.97	0.02		14.62 \pm 0.40
IC2524	9.95912	33.61961	-1	1462 \pm 13	0.87	0.23	61.8	15 \pm 0.49
UGC05349	9.96841	37.2928	7.8	1381 \pm 12	1.35	0.57	37.5	14.45 \pm 0.36
NGC3067	9.97253	32.36993	2.1	1473 \pm 4	1.31	0.49	104.3	12.73 \pm 0.12
PGC028991	10.01862	36.92261	4.8	1446 \pm 3	0.77	0.45	13.5	17.06 \pm 0.50
PGC029004	10.02065	37.07109	4.8	1463 \pm 2	0.7	0.18	174.8	16.80 \pm 0.46
SDSSJ100140.18+371538.3	10.02784	37.26055		1530 \pm 440	0.76	0.04		16.66 \pm 0.50
UGC05391	10.02805	37.2477	8.9	1568 \pm 10	1.3	0.56	167.7	15.24 \pm 0.52
UGC05393	10.02834	33.13635	8	1444 \pm 12	1.14	0.28	117	14.95 \pm 0.38
SDSSJ100142.11+371443.2	10.02837	37.24526		1567 \pm 369	1.2	0.55	163.6	16.79 \pm 0.50
UGC05394	10.02998	36.49881	6.2	1431 \pm 13	0.93	0.49	56.3	16.36 \pm 0.43
PGC2125269	10.05056	38.37724		1353 \pm 40	0.7	0.31	67.7	17.11 \pm 0.40
SDSSJ100309.92+323622.5	10.05276	32.60629		1562 \pm 96			123.3	
SDSSJ100429.42+365652.6	10.07484	36.94803		1602 \pm 61	0.59	0.17	59	18.15 \pm 0.50
PGC029347	10.10504	28.94493	-2.4	1362 \pm 7	0.82	0.03		14.54 \pm 0.09
UGC05446	10.10859	32.94659	5.9	1361 \pm 3	1.12	0.61	49.8	15.38 \pm 0.40
NGC3118	10.11988	33.02738	4.1	1342 \pm 4	1.32	0.67	38.6	14.34 \pm 0.35
PGC029522	10.14943	32.01043	4.7	1468 \pm 34	0.66	0.25	11.8	16.91 \pm 0.44
UGC05478	10.1588 s	30.1503	9.9	1377 \pm 4	1.19	0.03		14.75 \pm 0.06

Table B2. Galaxies in a box of 4 Mpc \times 4 Mpc centred on NGC 3607 in U376 with heliocentric radial velocity within $\pm 3\sigma$ of the group mean velocity given in the catalog of Ramella et al. (2002).

Galaxies	RA (J2000) (hours)	Dec. (J2000) (degrees)	Morph. type	Mean Hel. Vel. [km/s]	logD ₂₅ [arcmin]	logr ₂₅	P.A. [deg]	B _T mag
U376								
PGC031819	10.68599	21.36189		932 \pm 60	0.57	0.15	37.9	16.25 \pm 0.68
PGC1441580	10.69473	13.82499		1271 \pm 27	0.46	0.15	168.5	17.46 \pm 0.41
PGC031877	10.70009	12.33506	0.0	774 \pm 5	0.81	0.31	33.1	16.01 \pm 0.51
NGC3338	10.70210	13.74687	5.1	1299 \pm 2	1.09	0.24	97.0	11.44 \pm 0.21
SDSSJ104226.51+135725.7	10.70736	13.95720		1280 \pm 18	0.86	0.39	86.5	17.34 \pm 0.50
UGC05832	10.71348	13.45988	4.2	1216 \pm 3	1.04	0.16	86.3	14.48 \pm 0.70
PGC1439163	10.71455	13.74117		1145 \pm 5	0.40	0.20	48.0	18.40 \pm 0.50
PGC031937	10.71819	13.51109		1258 \pm 6			75.2	15.50 \pm 0.41
UGC05833	10.71835	20.42220	-2.0	1333 \pm 5	1.08	0.45	149.0	14.45 \pm 0.15
NGC3344	10.72531	24.92215	4.0	583 \pm 3	1.83	0.02		10.50 \pm 0.08
NGC3346	10.72747	14.87178	5.9	1257 \pm 9	1.42	0.08	118.6	12.45 \pm 0.34
NGC3351	10.73269	11.70355	3.1	778 \pm 2	1.86	0.21	9.9	10.58 \pm 0.12
SDSSJ104435.27+135622.7	10.74313	13.93964		633 \pm 31			116.5	
PGC2806914	10.74903	20.86190	9.0	1219 \pm 8				
PGC083326	10.74931	11.91611	10.0	871 \pm 4	0.60	0.36		17.36 \pm 0.36
PGC3090611	10.75273	15.44989		1219 \pm 3	0.68	0.14	119.2	17.23 \pm 0.45
PGC1733581	10.76385	25.35310	3.0	1418 \pm 41	0.68	0.54	33.4	17.87 \pm 0.37
AGC205287	10.77675	12.62639		957 \pm 8				
AGC205289	10.77686	12.43167		1006 \pm 8				
PGC083336	10.77813	12.32714	10.0	1030 \pm 5	0.82	0.13	10.8	16.91 \pm 0.42
AGC205290	10.77853	12.77972		915 \pm 8				
NGC3368	10.77936	11.81981	2.2	892 \pm 2	1.92	0.18	177.0	10.08 \pm 0.10
PGC4689210	10.78144	12.74444	10.0	640 \pm 5	0.90	0.12		18.45 \pm 0.57
PGC083338	10.78186	12.78795	10.0	928 \pm 8	0.70	0.15		18.20 \pm 0.29
PGC083339	10.78246	12.99925	10.0	832 \pm 4	1.08	0.30		17.63 \pm 0.34
PGC4689200	10.78356	12.95980	10.0	843 \pm 7	0.60	0.12		18.60 \pm 0.50
AGC205291	10.78414	12.22417		1018 \pm 8				
NGC3370	10.78445	17.27369	5.1	1281 \pm 4	1.39	0.24	143.5	12.29 \pm 0.30
AGC201972	10.78589	13.00472		834 \pm 8				
AGC205292	10.78594	13.05028		824 \pm 8				
AGC205293	10.78872	13.15583		806 \pm 8				
SDSSJ104720.05+122314.9	10.78891	12.38745		1146 \pm 45			30.8	
NGC3377A	10.78954	14.06997	8.9	573 \pm 2	1.16	0.02		14.40 \pm 0.11
AGC205294	10.79425	11.92861		971 \pm 5				
NGC3377	10.79510	13.98564	-4.8	684 \pm 11	1.59	0.32	37.2	11.13 \pm 0.17
AGC205295	10.79669	12.21639		978 \pm 8				
NGC3379	10.79711	12.58161	-4.8	908 \pm 6	1.69	0.06	71.0	10.23 \pm 0.17
SDSSJ104749.63+123432.6	10.79711	12.57587		922 \pm 25			178.3	
AGC205296	10.79722	13.12694		787 \pm 8				
AGC205297	10.80128	13.18750		794 \pm 8				
AGC205301	10.80344	12.06833		927 \pm 8				
AGC205302	10.80386	12.14167		917 \pm 8				
AGC205303	10.80442	12.29806		910 \pm 8				
NGC3384	10.80469	12.62890	-2.7	733 \pm 20	1.72	0.34	53.0	10.89 \pm 0.14
SDSSJ104819.74+123825.6	10.80550	12.64040		568 \pm 22			47.1	
NGC3389	10.80776	12.53310	5.3	1303 \pm 2	1.43	0.35	102.9	12.51 \pm 0.29
AGC205304	10.80789	12.42889		854 \pm 8				
AGC205305	10.80850	12.62611		648 \pm 8				
AGC205306	10.80919	12.49944		794 \pm 8				
AGC205307	10.81008	12.04667		924 \pm 8				
AGC205308	10.81200	13.26528		785 \pm 8				
PGC032348	10.81492	14.12450	-1.0	541 \pm 22	0.92	0.16	65.0	15.66 \pm 0.41
PGC032346	10.81579	12.19512	4.2	1323 \pm 3	0.87	0.22	14.4	15.70 \pm 0.63
PGC083348	10.81801	12.40737	5.4	1365 \pm 7	0.49	0.10	171.9	18.38 \pm 0.31
AGC205309	10.81883	12.37389		1342 \pm 8				
AGC205310	10.81994	12.49194		1379 \pm 8				
AGC205311	10.82017	12.19500		869 \pm 8				
PGC032371	10.82144	12.42196	9.0	1382 \pm 5	0.95	0.27	157.6	15.72 \pm 0.72
PGC032376	10.82206	12.37440	9.0	1346 \pm 6	0.89	0.00		17.00 \pm 0.35
PGC083352	10.82408	12.25776	-5.0	1321 \pm 3	0.60	0.15	29.6	17.26 \pm 0.69
AGC205197	10.82856	13.82806		1332 \pm 8				
AGC205313	10.83106	12.61139		774 \pm 8				
PGC1424345	10.83117	13.16179	10.0	764 \pm 6	0.60	0.09	81.0	18.98 \pm 1.08
AGC205314	10.83119	13.28667		787 \pm 8				
AGC205315	10.83131	12.53694		779 \pm 8				
AGC205316	10.83250	12.67028		776 \pm 8				
SDSSJ105001.79+134705.1	10.83384	13.78474		1311 \pm 1			129.8	
AGC205321	10.83414	13.10583		788 \pm 8				
AGC205322	10.83597	13.00583		797 \pm 8				
UGC05944	10.83861	13.27256	9.7	1073 \pm 27	0.97	0.02		15.27 \pm 0.44
UGC05945	10.84043	17.56435	9.8	1132 \pm 10	0.92	0.26	96.0	15.59 \pm 0.60
UGC05947	10.84177	19.64430	10.0	1253 \pm 12	1.09	0.24	25.0	14.92 \pm 0.08
UGC05948	10.84394	15.76333	10.0	1118 \pm 6	1.04	0.53	35.0	
NGC3412	10.84814	13.41218	-2.0	843 \pm 15	1.60	0.26	155.0	11.44 \pm 0.14

Table B2. Continue.

Galaxies	RA (J2000) (hours)	Dec. (J2000) (degrees)	Morph. type	Mean Hel. Vel. [km/s]	logD ₂₅ [arcmin]	logr ₂₅	P.A. [deg]	B _T mag
U376								
SDSSJ105053.31+132523.9	10.84815	13.42333		774±25			156.5	
SDSSJ105131.34+140653.1	10.85871	14.11477		832±53			30.2	
SDSSJ105204.79+150149.6	10.86798	15.03040		828±38			5.8	
PGC1388083	10.87208	11.04314		824±25	0.87	0.13	100.7	16.49±0.39
PGC032630	10.87261	17.93527	-0.4	1526±90	1.03	0.23	18.7	15.17±0.33
UGC05989	10.87551	19.79220	9.9	1126±5	1.16	0.49	125.1	14.25±0.33
SDSSJ105234.93+170841.8	10.87636	17.14495		1054±51	0.49	0.12	127.1	18.23±0.50
NGC3437	10.87657	22.93413	5.3	1276±11	1.37	0.46	118.8	12.59±0.38
AGC749324	10.88317	26.47278		1507±8				
NGC3443	10.88336	17.57361	6.6	1132±8	1.25	0.30	143.0	14.79±0.44
NGC3447	10.89000	16.77244	8.8	1069±3	1.53	0.24	25.6	14.54±0.68
SDSSJ105324.34+164735.4	10.89010	16.79327		1092±3	0.61	0.26	174.0	18.04±0.50
SDSSJ105329.58+164359.6	10.89155	16.73324		1017±65	0.62	0.09	160.0	17.84±0.50
NGC3447A	10.89158	16.78601	9.9	1094±7	1.17	0.28	105.8	16.39±0.50
UGC06014	10.89519	9.72750	8.0	1133±4	1.03	0.27	70.0	15.44±0.52
UGC06018	10.90159	20.64460	9.9	1291±4	1.02	0.03		
UGC06022	10.90427	17.80950	9.9	973±6	1.03	0.24	10.0	
NGC3454	10.90817	17.34407	5.5	1114±10	1.38	0.66	116.1	13.70±0.09
NGC3455	10.90863	17.28470	3.1	1106±5	1.36	0.20	68.5	14.32±0.24
NGC3457	10.91349	17.62111	-5.0	1159±5	0.99	0.02		12.97±0.24
UGC06035	10.92473	17.14170	9.9	1073±4	0.99	0.19	177.0	15.44±0.50
PGC032843	10.92901	17.00500	4.8	1143±29	0.80	0.04		15.24±0.38
PGC2806987	10.93228	12.33913	9.5	847±7	0.90	0.30		18.40±0.50
SDSSJ105603.00+234848.5	10.93417	23.81347		1278±50	0.54	0.26	175.9	18.50±0.50
PGC087256	10.93719	12.01109	10.0	990±4	0.84	0.20	153.5	17.18±0.59
SDSSJ105619.93+170505.9	10.93888	17.08503		954±3	0.45	0.04		18.52±0.50
SDSSJ105638.66+172301.2	10.94406	17.38381		941±3	0.58	0.29	156.2	18.19±0.50
PGC087257	10.96061	13.97881	10.0	1227±8			61.8	
PGC087170	10.98113	14.12973	5.0	684±12			105.3	
NGC3485	11.00067	14.84132	3.1	1434±5	1.34	0.03		12.67±0.27
NGC3489	11.00516	13.90119	-1.2	704±7	1.54	0.23	70.0	11.06±0.10
UGC06083	11.00660	16.69230	4.1	937±2	1.13	0.92	142.4	15.23±0.37
SDSSJ110047.14+165255.5	11.01311	16.88218		1146±39	0.55	0.16	103.4	18.13±0.50
UGC06095	11.01791	19.10020	10.0	1115±10	1.04	0.43	5.0	
PGC033270	11.03085	22.34454	3.1	1334±24	0.96	0.33	147.8	15.25±0.35
UGC06112	11.04311	16.73495	7.4	1038±6	1.28	0.52	120.1	14.79±0.52
NGC3501	11.04647	17.98957	5.9	1130±8	1.63	0.82	28.0	13.58±0.21
NGC3507	11.05705	18.13599	3.1	975±9	1.47	0.07		12.07±0.50
PGC087171	11.05733	16.01637	5.0	1228±6	1.01	0.43	15.9	16.85±0.50
PGC033447	11.07400	11.75599	10.0	778±8	1.11	0.49	144.1	15.91±0.39
SDSSJ110456.82+173830.5	11.08245	17.64173		918±40	0.80	0.33	114.1	17.44±0.50
PGC1724397	11.08688	25.06459		1482±289	0.45	0.19	129.8	17.75±0.43
PGC033523	11.09237	17.63963	-1.0	983±56	1.19	0.44	24.3	14.86±0.34
UGC06151	11.09896	19.82534	8.8	1331±3	1.18	0.02		14.90±0.09
NGC3524	11.10891	11.38537	0.1	1366±20	1.17	0.53	13.7	13.34±0.33
AGC215262	11.10981	12.23000		1606±8				
NGC3522	11.11124	20.08566	-4.9	1220±8	1.07	0.28	114.1	14.08±0.28
SDSSJ110651.09+173002.8	11.11418	17.50090		949±71	0.48	0.12	153.8	18.52±0.50
AGC749189	11.11589	26.90833		1159±8				
UGC06169	11.11761	12.06000	3.0	1553±5	1.22	0.75	1.4	14.54±0.34
UGC06171	11.11943	18.56943	9.9	1199±7	1.24	0.53	66.0	15.13±0.39
UGC06181	11.12962	19.54953	9.7	1169±2	1.02	0.18	48.0	15.54±0.36
PGC033816	11.15646	10.83412		1554±9	0.92	0.03		15.24±0.38
NGC3547	11.16553	10.72052	3.1	1580±2	1.24	0.35	6.2	13.20±0.12
PGC033905	11.17365	10.12589	9.0	1322±11	0.95	0.23	117.9	15.92±0.59
PGC033981	11.18180	9.62186	3.1	1577±10	0.75	0.15	107.0	15.49±0.50
PGC087172	11.20437	16.75397	10.0	1205±9	0.95	0.35		17.40±0.50
AGC219368	11.20606	24.07750		761±8				
[RGK2003]J111223.17+134248.9	11.20643	13.71370		630±99				
PGC087259	11.20881	16.28964	-5.0	1250±71	0.91	0.31	147.3	16.89±0.50
UGC06248	11.21439	10.20003	9.9	1286±3	1.05	0.10	53.1	23.43±0.50
AGC215280	11.22119	15.40778		1479±8				
UGC06258	11.23050	21.52043	9.9	1454±3	0.92	0.51	172.7	15.34±0.40
SDSSJ111350.75+095739.4	11.23078	9.96087		1610±5	0.35	0.06	74.3	18.55±0.50
AGC215387	11.23742	12.77944		578±8				
PGC1487160	11.24033	15.53389		861±30	0.75	0.22	92.7	17.05±0.50
NGC3592	11.24093	17.25999	5.3	1302±4	1.33	0.57	117.7	14.47±0.30
NGC3593	11.24361	12.81765	-0.4	630±3	1.67	0.40	91.2	11.85±0.12
SDSSJ111445.01+123851.7	11.24584	12.64759		628±8	0.72	0.24	95.7	17.51±0.50
NGC3596	11.25173	14.78694	5.2	1192±2	1.55	0.02		11.79±0.08
SDSSJ111506.95+144708.3	11.25192	14.78565		1203±35			179.9	
SDSSJ111516.15+144154.9	11.25450	14.69867		1092±45			17.5	
NGC3599	11.25750	18.11033	-2.0	837±20	1.38	0.04		12.88±0.08
SDSSJ111532.38+143438.4	11.25899	14.57736		1133±8	0.55	0.09	145.4	17.84±0.50

Table B2. Continue.

Galaxies	RA (J2000) (hours)	Dec. (J2000) (degrees)	Morph. type	Mean Hel. Vel. [km/s]	logD ₂₅ [arcmin]	logr ₂₅	P.A. [deg]	B _T mag
U376								
NGC3605	11.27963	18.01717	-4.5	675±15	1.10	0.24	19.1	13.16±0.28
UGC06296	11.28086	17.79847	8.0	976±2	1.11	0.48	168.7	14.18±0.41
NGC3607	11.28182	18.05190	-3.2	930±3	1.66	0.06	120.0	10.93±0.17
NGC3608	11.28304	18.14854	-4.8	1211±20	1.50	0.08	80.0	11.57±0.26
IC2684	11.28363	13.09921		591±11	0.88	0.13	171.2	15.78±0.61
SDSSJ111702.67+100836.1	11.28408	10.14330		1765±5	0.75	0.43	31.6	17.72±0.50
AGC215386	11.29750	13.98222		871±8				
PGC034522	11.29945	17.44132		766±2	0.95	0.06	157.3	15.10±0.29
SDSSJ111803.87+101439.9	11.30107	10.24441		957±65	0.54	0.18	118.5	18.33±0.50
PGC034537	11.30167	18.79814	4.9	1140±7	0.73	0.04		16.35±0.38
UGC06320	11.30481	18.84708	8.0	1122±4	1.13	0.03		13.83±0.41
PGC086629	11.30593	17.69740	9.8	1055±5	0.89	0.00		
UGC06324	11.30614	18.73836	-1.9	1083±56	1.14	0.33	166.8	14.77±0.32
AGC215389	11.30797	14.30056		917±8				
AGC215392	11.30933	14.53083		909±8				
SDSSJ111842.18+123341.7	11.31173	12.56175		979±58	0.73	0.15	152.8	17.47±0.50
AGC215393	11.31467	13.40667		862±8				
AGC215396	11.31500	12.89472		581±8				
AGC215397	11.31525	14.21556		909±8				
NGC3623	11.31551	13.09294	1.0	806±5	1.88	0.59	173.0	10.14±0.13
AGC215398	11.31819	12.75528		753±8				
AGC215400	11.31894	12.65194		753±8				
AGC215401	11.32006	13.59250		834±8				
AGC215286	11.32019	14.32778		998±8				
SDSSJ111914.39+115707.7	11.32066	11.95203		861±4	0.87	0.30	94.1	17.01±0.50
SDSSJ111915.87+141724.8	11.32108	14.29024		728±36			171.1	
SDSSJ111921.39+140431.6	11.32262	14.07550		485±132	0.65	0.27	144.7	18.39±0.50
AGC215402	11.32392	13.23389		772±8				
PGC1367320	11.32447	9.59562		990±6	0.62	0.31	117.7	17.81±0.55
AGC215403	11.32511	12.56361		716±8				
AGC215405	11.32592	12.51417		695±8				
AGC215406	11.32608	13.85944		984±8				
AGC215407	11.32711	12.39333		655±8				
AGC215287	11.32919	15.50222		1334±8				
AGC215409	11.33175	12.87528		678±8				
AGC215410	11.33303	13.29000		785±8				
UGC06341	11.33350	18.26050	7.9	1611±42	1.00	0.44	152.1	16.12±0.39
NGC3626	11.33438	18.35704	-0.9	1480±5	1.47	0.18	156.3	11.81±0.23
SDSSJ112009.38+133555.3	11.33594	13.59866		650±33				
NGC3627	11.33750	12.99099	3.1	721±2	2.01	0.35	173.0	9.74±0.20
NGC3628	11.33804	13.58876	3.1	846±2	2.04	0.51	103.3	9.97±0.18
AGC215411	11.34086	12.86778		646±8				
NGC3629	11.34216	26.96328	5.9	1508±4	1.25	0.19	34.5	13.12±0.49
PGC1534499	11.35698	17.51034	9.0	979±57	0.92	0.25	145.0	16.46±0.50
AGC215412	11.36328	13.61861		908±8				
[RGK2003]J112216.25+205158.7	11.37117	20.86628		810±60				
PGC2806917	11.37124	20.87560	10.0	810±8				
IC2763	11.37180	13.06512	6.0	1569±2	1.16	0.57	98.2	15.14±0.35
SDSSJ112223.18+130440.1	11.37311	13.07784		1078±2	0.94	0.47	90.7	17.08±0.50
AGC215413	11.37317	13.64583		905±8				
PGC1398872	11.37317	11.79393		1571±4	0.53	0.21	111.1	17.98±0.45
PGC1420152	11.37333	12.97956		626±26	0.63	0.05	142.1	17.31±0.49
PGC1407849	11.38074	12.34474		1544±6	0.56	0.03		17.25±0.35
NGC3655	11.38186	16.59003	5.0	1453±13	1.18	0.16	31.8	12.32±0.07
IC2782	11.38205	13.44105	8.0	860±24	0.97	0.05	22.6	15.12±0.41
AGC215290	11.38308	12.46056		1613±8				
PGC086673	11.38316	17.47390	10.0	1383±4	0.79	0.00		
AGC215414	11.38642	13.70556		878±8				
HIPASSJ1122+13	11.38700	13.71541	10.0	883±10				
IC2787	11.38863	13.62967	6.0	708±27	0.90	0.04		15.70±0.45
SDSSJ112337.61+125344.8	11.39377	12.89597	9.0	666±6	0.76	0.20	158.6	17.15±0.50
NGC3659	11.39594	17.81839	7.7	1284±11	1.29	0.28	59.2	12.92±0.48
PGC091112	11.40367	26.24551	5.6	1483±11	0.78	0.73	61.8	17.31±0.50
AGC729579	11.40481	25.71056		1523±8				
NGC3666	11.40726	11.34195	5.2	1060±2	1.54	0.54	97.5	12.69±0.11
AGC215415	11.40950	12.67778		1004±8				
PGC1480186	11.41236	15.27553		1125±6	0.84	0.44	5.9	17.45±0.50
PGC035087	11.41717	17.08572	9.0	1208±5				
PGC035096	11.41966	16.88431	9.5	1021±3	0.76	0.15	147.0	16.12±1.17
AGC749436	11.42331	23.91889		1024±8				
IC0692	11.43153	9.98722	1.9	1158±4	0.88	0.16	117.7	14.18±0.35
NGC3681	11.44161	16.86328	4.0	1240±3	1.24	0.01		12.42±0.16
AGC215296	11.44867	14.83417		913±8				
NGC3684	11.45311	17.03018	4.0	1159±6	1.36	0.18	126.2	12.31±0.11

Table B2. Continue.

Galaxies	RA (J2000) (hours)	Dec. (J2000) (degrees)	Morph. type	Mean Hel. Vel. [km/s]	logD ₂₅ [arcmin]	logr ₂₅	P.A. [deg]	B _T mag
U376								
NGC3686	11.46220	17.22409	4.1	1157±3	1.46	0.12	22.7	12.00±0.07
NGC3691	11.46928	16.92044	3.0	1078±10	1.17	0.15	22.0	12.64±0.17
NGC3692	11.47342	9.40753	3.1	1719±4	1.51	0.63	93.4	13.03±0.55
PGC086634	11.48088	18.28267	9.5	1303±9	1.01	0.15		17.10±0.50
PGC035380	11.48730	20.58080	10.0	1412±33	0.31	0.18		16.31±0.16
IC0700	11.48759	20.58336	4.2	1415±6	0.97	0.31	70.9	14.09±0.23
PGC035384	11.48788	20.58566	10.0	1420±35	0.48	0.04		17.23±0.14
PGC035385	11.48793	20.58816	10.0	1670±50	0.39	0.35	54.4	18.73±0.19
SDSSJ112934.60+104835.4	11.49295	10.80987		744±46	0.55	0.06	160.8	17.74±0.50
PGC035426	11.49847	16.42957		1067±5				
NGC3705	11.50209	9.27667	2.4	1019±3	1.63	0.39	121.0	11.76±0.10
PGC2807141	11.51478	14.14596	10.0	878±1				
SDSSJ113108.88+133413.4	11.51912	13.57052		1013±7			114.4	
PGC035565	11.53386	14.61087	4.8	1123±7	0.79	0.41	85.6	17.03±0.50
PGC1468083	11.56391	14.82472	3.2	1129±6	0.54	0.21	8.2	17.75±0.50
SDSSJ113350.91+140315.0	11.56414	14.05420		933±2			93.1	
IC2934	11.57212	13.32139	4.9	1196±6	0.87	0.29	152.9	15.34±0.59
PGC2807142	11.58147	11.02016	10.0	882±2				
SDSSJ113456.50+161452.5	11.58237	16.24797		1135±4	0.54	0.13	137.9	17.80±0.50
SDSSJ113708.79+131504.9	11.61912	13.25120		983±5	0.83	0.47	38.9	17.50±0.50
PGC086675	11.62536	18.59347	9.0	958±60	0.84	0.00		
UGC06594	11.62696	16.55621	6.4	1043±5	1.33	0.74	132.3	14.89±0.37
UGC06599	11.62847	24.13256	9.9	1569±2	0.99	0.45	172.0	16.61±0.50
NGC3773	11.63695	12.11216	-2.0	985±4	1.09	0.10	160.0	13.51±0.53
PGC1448560	11.68241	14.07445		910±7	0.83	0.49	129.0	17.12±0.50
NGC3810	11.68300	11.47120	5.2	993±2	1.52	0.17	31.6	11.27±0.10
UGC06655	11.69739	15.97359	-1.0	740±4	0.83	0.21	31.0	14.93±0.65
UGC06669	11.70516	14.99519	9.9	1022±2	1.12	0.29	68.8	
UGC06670	11.70814	18.33374	9.9	922±1	1.18	0.47	154.3	13.39±0.28
PGC036412	11.71957	14.22419	10.0	1015±1				
PGC1393002	11.72417	11.39835		898±7	0.57	0.06	164.6	16.82±0.48
PGC2806928	11.80454	18.64242	10.0	976±6	0.52	0.00		
SDSSJ114843.14+171053.1	11.81197	17.18155		1092±337	0.70	0.32	96.2	17.91±0.50
SDSSJ114850.14+102655.9	11.81393	10.44876		753±102				
UGC06782	11.81593	23.83769	9.8	523±16	1.24	0.00		15.16±0.16
PGC1528400	11.81822	17.25570		623±29	0.38	0.13	63.9	18.49±0.54
NGC3900	11.81928	27.02194	-0.2	1800±2	1.41	0.31	1.5	12.29±0.07
SDSSJ114925.75+253700.4	11.82382	25.61673		1799±8	0.48	0.13	155.8	18.34±0.50
SDSSJ114931.03+151539.7	11.82528	15.26094		857±29			148.9	
SDSSJ114957.11+161743.6	11.83254	16.29550		1188±45	0.52	0.22	154.7	18.13±0.50
PGC036976	11.83409	15.02331	4.6	751±2	0.71	0.17	89.0	15.76±0.54
NGC3912	11.83459	26.47946	3.1	1787±3	1.18	0.35	3.3	13.34±0.51
PGC1739846	11.84440	25.52629	4.8	1819±3	0.91	0.49	152.3	16.58±0.36
PGC037048	11.84887	14.59490		1008±5	0.54	0.21	51.9	16.66±1.22
PGC037162	11.86718	13.87873	4.4	967±4	0.78	0.10	41.7	15.28±0.41
SDSSJ115220.20+152736.2	11.87228	15.46006		787±6	0.79	0.48	52.3	18.35±0.50